Key Points:
- Extension of the two-source model permits reliable half-hourly simulations of transpiration fluxes in three tidal mangrove ecosystems
- Suppression of transpiration under high temperatures is stronger in mangroves than in well-watered ecosystems
- The narrow temperature tolerance range and evident tidal effects imply potential further effects of climate change on mangrove transpiration

Supporting Information:
- Supporting Information S1

Correspondence to:
X. Lee and G. Lin,
lingh@tsinghua.edu.cn;
xuhui.lee@yale.edu

Evapotranspiration Characteristics Distinct to Mangrove Ecosystems Are Revealed by Multiple-Site Observations and a Modified Two-Source Model

Jie Liang[1,2,3] (iD), Zhongwang Wei[2,5] (iD), Xuhui Lee[2,6] (iD), Jonathon S. Wright[1,3] (iD), Xiaowei Cui[1,3,4], Hui Chen[1,7] (iD), and Guanghui Lin[1,3,4] (iD)

[1]Ministry of Education Key Laboratory for Earth System Modeling, Department of Earth System Science, Tsinghua University, Beijing, China, [2]School of Forestry and Environmental Studies, Yale University, New Haven, CT, USA, [3]Joint Center for Global Change Studies, Beijing, China, [4]Division of Ocean Science and Technology, Graduate School at Shenzhen, Tsinghua University, Shenzhen, China, [5]River and Environmental Engineering Laboratory, Department of Civil Engineering, The University of Tokyo, Tokyo, Japan, [6]Yale-NUIST Center on Atmospheric Environment, Nanjing University of Information Science & Technology, Nanjing, China, [7]College of Life Science, Yangtze University, Jingzhou, China

Abstract A quantitative accounting of how mangrove ecosystems respond to tidal perturbations is needed to anticipate changes in these ecosystems when sea level rises. Here we use long-term field observations and a two-source ecohydrological model to reveal specialized characteristics of evapotranspiration (*ET*), soil surface evaporation (*E*), and canopy transpiration (*T*) in three subtropical mangrove ecosystems in southeastern China. Average wintertime *ET* observed in these three mangrove forests (2.6 mm day^{-1}) was consistent with values for semiarid ecosystems, while average summertime *ET* (6.2 mm day^{-1}) approached that observed in rainforests. By contrast, *T* fluxes were small year-round, averaging 1.3 mm day^{-1} in winter and 2.5 mm day^{-1} in summer. Combining our results with measurements from three Florida mangroves, observed values of *T* ranged from 350 to 870 mm year^{-1}, varying primarily with salinity, while *T/ET* increased exponentially from 30% to 70% with rising leaf area index. Simulations of half-hourly *ET* and *T* using a modified two-source model were highly correlated with eddy covariance observations of *ET* (*I*, index of agreement >0.93 at all three sites) and sap flow gauge-based estimates of *T* (*I* = 0.93 at the Yunxiao site). Variations of *T* in mangrove ecosystems are distinguished from those in terrestrial forests mainly by the sensitivity of stomatal conductance to leaf temperature, with tidal and salinity effects superimposed. Our modified model accounts for these effects and therefore holds promise for improving our understanding of how mangrove ecosystems may respond to changing stress conditions under global warming and sea level rise.

1. Introduction

Situated in the coastal regions of the tropics and subtropics, mangrove forests are subject to several unusual sources of water and temperature stress (Ball, 1988). Unlike freshwater vegetated systems, mangrove forests must obtain water from saline soils. The high carbon and energetic costs of salt exclusion during water uptake require mangrove trees to use water conservatively despite the abundance of water in coastal areas (Ball et al., 1988; Beerling & Franks, 2010). The conservative water use characteristic of mangroves is reflected in adaptive changes of transpiration rates with salinity: Transpiration rates for mangrove forests in hypersaline habitats are as low as those observed in arid ecosystems (Alongi & Mukhopadhyay, 2015; Krauss et al., 2007), but values in hypohaline habitats are as high as those observed in evergreen forests. Despite these limitations, mangrove ecosystems are highly productive, with annual primary production comparable to tropical humid evergreen forests and coral reefs (Alongi, 2014; Barr et al., 2010; Cui et al., 2018; Lu et al., 2017). These unique features motivate us to study the dynamic patterns of gas exchange in mangrove ecosystems through which mangroves are able to assimilate large amounts of atmospheric carbon with relatively little water loss. Moreover, because they directly interact with coastal waters, mangrove forests may be particularly sensitive to changes in sea level, intensity variability of rainfall, and the frequency of extreme events (Alongi, 2008; Alongi, 2015; Barr et al., 2009; Barr et al., 2012; Gilman et al., 2007; Gilman et al., 2008). Quantitative accounting of water exchange between mangrove ecosystems and the

atmosphere is therefore a priority as we work to anticipate how mangrove ecosystems may adapt to future climate change.

Current hydrological models are parameterized to depend largely on the atmospheric state and can be applied to most land cover types with careful adjustment (Choi et al., 2012). However, models developed for terrestrial systems typically do not account for the effects of stressors unique to tidal mangrove forests, including periodic flooding and salinity-induced water stress. For example, the effects of tidal perturbations on surface energy fluxes and transformations (Barr, Fuentes, et al., 2013; Sobrado, 2007) and the effects of salinity on light use efficiency (Barr, Engel, et al., 2013; Cui et al., 2018; Krauss et al., 2008) and stomatal or mesophyll conductance (Lin & Sternberg, 1992; Parida et al., 2004; Reef & Lovelock, 2015; Sobrado, 2000; Sobrado, 2005) may distinguish the transpiration capacities of mangrove forests from those of terrestrial forests (Clough & Sim, 1989; Collatz et al., 1991). Some observations have suggested that hypersaline conditions can induce a sharp reduction of stomatal conductance under intense solar irradiance (>500 W m^{-2}) via inhibition of photosynthesis when more light is absorbed than can be used (Barr et al., 2009; Bjorkman et al., 1988; Lovelock & Ball, 2002; Lovelock & Winter, 1996; Osmond, 1994; Sobrado & Ball, 1999). The dissipation of excess light energy within a leaf tends to increase the leaf water deficit by raising the leaf temperature and can thus intensify stomatal closure under hypersaline conditions. Yet these processes governing the response of stomatal conductance to salinity via light use efficiency are typically neglected in general terrestrial models based on local climatic variables (Choi et al., 2012; Collatz et al., 1991; Wei et al., 2018). As the rate of transpiration is determined by leaf stomatal conductance (Farquhar et al., 1989), accurate estimates of transpiration in mangroves require reliable representations of how leaf conductance responds to variations in the saline habitat.

Ronda et al. (2001) successfully implemented a conductance submodule based on plant physiological processes that was incorporated into a two-source ecohydrological model (Shuttleworth & Wallace, 1985) for ecosystems with sparse vegetation cover. In the two-source model, energy balance constraints are applied separately to the soil and canopy of sparse, heterogeneous natural ecosystems to calculate the associated water and heat transfers (Jacobs, 1994; Ronda et al., 2001; Wei et al., 2018). The canopy conductance model represents vapor fluxes from the leaf interior to a reference height via a sequence of resistance analogues, including canopy resistance and aerodynamic resistance (Shuttleworth & Wallace, 1985). Canopy resistances are coupled with a plant physiology scheme, allowing different kinds of stress experienced by the plant to be expressed as changes in the effective resistance. After some modifications, the plant physiology submodule may be similarly adapted to quantify the joint effects of tidal and temperature fluctuations on transpirations in mangrove ecosystems and thus to predict how these ecosystems may respond to climate change and associated sea level rise.

Given the unique nature of mangrove ecosystems, in this study, we aim to (1) understand specialized characteristics of ecosystem-scale water fluxes in tidal mangroves and (2) modify the two-source model to reliably represent the stresses and features that characterize mangrove ecosystems, including tidal fluctuations, salinity tolerance, and potential high-temperature adaptations.

2. Materials and Methods

2.1. Study Sites

The data used in this study were collected from mangrove ecosystems at three sites (Table 1): Gaoqiao (GQ), Leizhou (LZ), and Yunxiao (YX). The GQ and LZ sites are respectively located in the western and eastern parts of the Zhanjiang Mangrove National Nature Reserve, Guangdong, the largest natural mangrove reserve in China (Chen et al., 2009). The YX site is located in the Zhangjiangkou Mangrove National Nature Reserve, in Fujian Province, China. The forest canopy heights are approximately 2.5 to 4.0 m at GQ, 8 to 15 m at LZ, and 3 to 4 m at YX, with average leaf area index (*LAI*) values of 2.9, 2.8, and 2.5 m^2 m^{-2}, respectively. Annual rainfall amounts at GQ, LZ, and YX were 1,560, 1,480, and 1,240 mm during 2009–2017 (MSWEP V2 global three hourly 0.1° precipitation, Beck et al., 2019), with two distinct peaks during May–August and September–November. Annual mean air temperatures (T_a) during the measurement periods were 22 °C at GQ, 23 °C at LZ, and 21 °C at YX, with daily maximum T_a peaking at around 40 °C in August and daily minimum T_a falling to around 5 °C in January. All three sites experience semidiurnal tides, with two high tides per day on most days. The maximum tides reach approximately 2.8 m at GQ, 1.6 m at LZ, and 1.2 m at YX. Salinity

Table 1
Characteristics of Mangrove Ecosystems at Study Sites

Site	Location	Dominant species	Canopy height (m)	LAI (m^2 m^{-2})	Rainfall (mm)	MT (°C)	Tide Range (m)	Tide Salinity (PSU)
LZ	20.9400°N, 110.1628°E	*S. apetala*	8–15	2.8	1,480	23	1.6	0–54
GQ	21.5674°N, 109.7565°E	*B. gymnorrhiza* *A. corniculatum* *A. marina*	3.5–4	2.9	1,560	22	2.8	2–35
YX	23.9243°N, 117.4156°E	*K. obovata* *A. corniculatum* *A. marina*	3–4	2.1–2.6 1.2–2.8 1.7–2.2	1,240	21.1	1.2	2–24

Note. Tidal range is calculated as the maximum minus the minimum. MT = mean annual air temperature; *LAI* = plant area index, measured by hemispherical canopy photography using a digital camera with a fish-eye lens.

fluctuates seasonally, with measured minimum values of approximately 2–15 practical salinity units (PSU) during October–November and maximum values of 25–54 PSU during April–June at GQ and LZ. The April–June annual maximum salinity is slightly less at the YX site, with an average value of only about 24 PSU during 2010 to 2012 (supporting information Figure S1D).

2.2. Data Collection

2.2.1. Water Flux Measurements and Data Processing

Each of the three sites hosts one observational tower (Figure S2), with the towers reaching heights of 14 m at GQ, 20 m at LZ, and 14.7 m at YX. *ET* fluxes were measured using the eddy covariance (EC) approach, which requires an open-path infrared carbon dioxide and water vapor analyzer (LI-7500; Li-Cor, Inc., USA) and a 3-D sonic anemometer (CSAT3; Campbell Scientific, Inc., USA). Flux data were recorded at high frequency (10 Hz) and logged at 30-min intervals using a data logger (CR1000; Campbell Scientific, Inc., USA). According to the height of the local vegetation canopy (Table 1), EC systems were mounted at 8.6 m above ground level at GQ, 18 m above ground level at LZ, and 8 m above ground level at YX. Microclimate parameters including air temperature and humidity (HMP45AC; Vaisala, Inc., Finland), wind speed (010C; Met One Instruments, Inc., USA), and wind direction (020C; Met One Instruments, Inc., USA) were measured at heights of 2.6, 7.4, and 14.0 m at GQ, 3.0 and 18.0 m at LZ, and 3.0 and 12.6 m at YX. Solar radiation, photosynthetically active radiation (PAR), and net radiation were measured by using a pyranometer sensor (LI-200SZ; Li-Cor, Inc., USA), a PAR quantum sensor (LI-190SZ; Li-Cor, Inc., USA), and a four-component net radiation sensor (NR01; Hukseflux Thermal Sensors, Inc., USA), respectively, at all three sites. All three sets of measurements were logged as 30-min averages using a second data logger. Rainfall amounts at all three sites were measured using automated devices (TE525MM, Texas Electronics, Inc., USA). Tidal gauge instruments were used to record water temperature, water level, and water salinity (YSI, Yellow Springs, USA) every 10 min at a location 2 m away from the tower in each of the three mangrove ecosystems. Soil heat flux measurements were collected in surface soil at 5-cm depth (HFT-3, REBS, USA), along with measurements of soil temperatures (CS107, CSI, USA) at depths 5, 10, and 20 cm below the soil surface. EC processing consisted of three steps including (1) flux calculation and correction through axis rotation, ultrasonic correction, and frequency filtering in sequence; (2) data quality control using footprints and friction velocities; and (3) gap filling using the MDS gap-filling algorithm (mean diurnal variation—lookup tables based) in the R package REddyProc. The distributions of mangrove species (Table 1) at each site are complex; however, the height differences among species at each site are small (<1 m), so the underlying surfaces within each tower's footprint are approximately flat. Detailed identification of mangrove footprint and the EC data procedures have been provided by Liu (2015), Cui (2018), and Cui et al. (2018). Site-level data were collected from 2010 through 2016 at the GQ site, from 2015 through 2017 at the LZ site, and 2010 through 2012 at the YX site. Before gap filling, missing data fractions for EC-based daytime latent heat fluxes (LE) were 36% at GQ, 11% at LZ, and 4% at YX.

2.2.2. Estimating Stand Canopy Transpiration

Measurements of sap flux were made from 4 June 2011 to 30 June 2012 at YX only. Approximately 12% of these measurements were unusable due to wet probes or lack of power. A quadrat survey at YX indicated that diameters at breast height (DBH) of mangrove trees were consistently less than 10 cm (Yan et al., 2016). We

therefore grouped the mangrove trees into three size classes based on diameter: small (20- to 40-mm DBH), medium (40- to 70-mm DBH), and large (80- to 100-mm DBH). Before conducting the sap flux experiment, sapwood depths were determined by destructive sampling of representative trees from the two dominant mangrove species and the three size classes. Fresh cores showed differences in the color or transparency of sapwood and heartwood reflecting differences in water content (Table S1). Pairs of 2-mm-diameter probes were embedded to identical depths of sapwood in the tree trunks at heights 1.3 to 1.5 m above the maximum tide level (Table 1). Pairs of probes were spaced at vertical distances of 10 to 15 cm and were installed on the north-facing sides of tree trunks to avoid direct solar radiation. Both the heated upper probe and the unheated lower probe were wrapped in aluminum foil. Three commercially available probes (TDP-10, TDP-20, and TDP-50; Dynamax, Inc., Houston, Texas, USA) were inserted at radial depths of 10, 20, and 40 mm, respectively. These probes were then connected to CR1000 dataloggers (Campbell Scientific, Logan, Utah, USA) to monitor flow rates at different radial depths. For small, medium, and large trees, two to three individuals in each size class of two dominant mangrove species, *Kandelia obovata* and *Avicennia marina*, were selected. Data collected for these selected individuals were then extrapolated to the entire mangrove canopy according to the distribution ratios of these typical species in representative quadrats within the footprint of the eddy flux tower (Table S1). After peeling off two pieces of bark, one pair of TDP-10 probes were inserted to 10-mm xylem radial depth in each small tree to capture the flow rate at 0–10 mm in small-diameter trees. One pair of TDP-20 probes were inserted to 15-mm radial depth in each medium tree to capture the flow rate at 0–20 mm in medium-diameter trees. Finally, one pair of TDP-20 probes and one pair of TDP-50 probes were inserted to 15- and 30-mm radial depths in each large tree to test flow rates at 0–20 and 20–40 mm of large-diameter trees, respectively.

Sap fluxes at each depth (J_s, g H_2O m^{-2} sapwood s^{-1}) are determined by temperature differences between the heated and unheated probes relative to zero-flow conditions, as formalized in the equation (Granier, 1987; Granier et al., 1996; Krauss et al., 2007):

$$J_s = 1,190 \left(\frac{\Delta T_{\max} - \Delta T}{\Delta T} \right)^{1.23}, \tag{1}$$

where $\Delta T_{\max}$ is the maximum temperature difference between the probes. In this study, $\Delta T_{\max}$ is regarded as daily maximum value of ΔT. Individual tree water usage (F_{tree}: g H_2O s^{-1}) is then determined by:

$$F_{\text{tree}} = \sum_{i=1}^{n} (J_{si} \times SA_i), \tag{2}$$

with i an integer index corresponding to the ith radial depth into the sapwood. Sap flow at the first depth is thus represented by J_{s1}, and SA_i represents the area of sapwood corresponding to the depth range (SA, unit: m^2) sampled by the heating probe at the ith radial depth (Table S1).

We then upscaled the water fluxes for individual trees to estimate the stand canopy transpiration latent enthalpy flux (λT; unit: W m^{-2}) based on the equation (Cermák, 1989; Hatton & Wu, 1995; Soegaard & Boegh, 1995; Vertessy et al., 1995; Bloemen et al., 2016):

$$\lambda T = \lambda \frac{\sum_{j=1}^{m} \left((F_{\text{tree}})_j / LAI_j \right)}{A} LAI_\mu, \tag{3}$$

where λ is the latent enthalpy of vaporization at 20 °C ($\lambda \approx 2,466$ J g^{-1}), A is the ground area occupied by the stand (unit: m^2), $(F_{\text{tree}})_j$ is the mean sap flux density of trees in class j ($m = 2$ species × 3 circumference classes in this study), LAI_μ is the mean leaf area index of the mangrove forest, and LAI_j is the mean leaf area index for class j. The LAI values in Table S1 were measured by hemispherical canopy photography using a digital camera with a fish-eye lens (Coolpix995, Nikon Corporation, Tokyo, Japan).

Our observations of canopy transpiration were inferred by upscaling sap flow measurements from individual trees to estimate stand transpiration. Such upscaling approaches depend crucially on quadrat surveys (Granier et al., 1996). Although we have done our best to sample representative quadrats within the eddy tower footprint, errors in the quadrat survey and variations in wind direction may cause uncertainties in estimations of stand transpiration using the sap flow method (Köstner et al., 1998; Krauss, Duberstein, et al., 2015). Our calculations of T strictly follow the standard sap flow method; we therefore assume that they are reliable within that context.

2.2.3. *LAI* Data Processing

The leaf area index (*LAI*) is an important input variable in this model. We used time-series *LAI* values from MODIS retrievals in grid h28v06 for all three sites in this study. These data have a 16-day temporal resolution and a 500-m spatial resolution. We linearly interpolated the 16-day data in time to get daily estimates of *LAI*, which are then assumed to be constant across all 30-min time steps on any given day. As *LAI* estimates based on satellite images are subject to large uncertainties, we calibrated MODIS-based *LAI* values using direct field measurements of *LAI* collected during this and other studies (Chen et al., 2017; Clough et al., 1997; Wen, 1999). The calibration equation at YX (sparse crown closure with multilayer leaves) was $Y = 1.064X + 0.9107$ (*X* representing MODIS-based *LAI*), while that at LZ and GQ (dense crown closure with approximately single-layer leaves) was $Y = 2.164X + 0.9107$.

2.3. Statistical Analysis

Meteorological variables were aggregated as 30-min averages ($X_{30\ \text{min}}$) for investigating diurnal variability and as daily averages (X_{day}) weighted by 30-min variations in incoming short-wave solar radiation ($K_{\downarrow}$) for investigating seasonal variability (Barr et al., 2010) to emphasize values associated with larger fluxes of solar radiation: $X_{\text{day}} = \sum_{i=1}^{48} \left(\frac{(K_{\downarrow 30\ \text{min}})_i}{\sum_i^{48}(K_{\downarrow 30\ \text{min}})_i} (X_{30\ \text{min}})_i \right)$. Daily values of salinity and water level are expressed as daily maxima rather than daily means. Fluxes such as λET and λT are summed for use in the seasonal analysis, with enthalpy fluxes in units of W m^{-2} converted to moisture fluxes in units of mm day^{-1}: $Y_{\text{day}} = \frac{1.8}{\lambda} \times \sum_i^{48} (Y_{30\ \text{min}})_i$. Before summing flux variables, gaps in the EC data were filled using the REddyProc package in R to ensure temporal consistency. Annual gross fluxes (unit: mm year^{-1}) were calculated by summing the daily fluxes.

The performance of the modified two-source model is evaluated via two metrics: index of agreement (*I*) and root-mean-square error (RMSE). Both metrics are calculated relative to 30-min EC observations of *ET* and 30-min sap flow-based estimates of *T*. The metrics are defined as follows:

$$I = 1 - \frac{\sum_{i=1}^{N}(S_i - M_i)^2}{\sum_{i=1}^{N}\left(|S_i - \overline{M}| + |M_i - \overline{M}|\right)^2}, \tag{4}$$

$$\text{RMSE} = \left[\frac{1}{N} \sum_{i=1}^{N}(S_i - M_i)^2 \right]^{1/2}, \tag{5}$$

where *N* is the total number of observations, S_i and M_i are the simulated and measured values, respectively, and $\overline{S}$ and $\overline{M}$ are the corresponding means. To clarify the effects of key parameters on the model predictions, sensitivity tests examining the response of output variables to variations in selected model parameters were conducted following the method proposed by Beven (1979). The sensitivity coefficient (*SC*) of the target model output variable *O* (*T*, *ET*, or *T/ET*) conditional on a specified model input parameter *P* is determined as:

$$SC = \frac{1}{N} \sum_i^{N} \frac{\left(O_i^* - O_i\right)}{P_i^* - P_i} \frac{P_i}{O_i}, \tag{6}$$

where *N* is the number of output variables in *O*, the subscript *i* is the *i*[th] output variable of *N* variables in *O*, and the superscript "*" denotes a provisionally assumed value of *P* or a modeled value of *O* based on that assumed value of *P*. A positive *SC* value of 0.1 means that a 1% increase in the input parameter is expected to induce a 0.1% increase in the simulated variable.

To clarify uncertainties in the model simulations, a Monte Carlo uncertainty analysis was conducted for key input parameters. The parameters for the modified two-source model were calibrated by field observations from the published literature (discussed in section 3.3). The performance of this model was then validated using EC-based measurements of *ET* (at all three mangrove forests) and sap flow-based measurements of *T* (at YX only). Furthermore, data collected from other field observations and greenhouse experiments have been pooled to validate the relationship between modeled stomatal conductance and salinity.

3. Two-Source Model in Mangrove Ecosystems

3.1. Surface Energy Balance

The two-source model is used to calculate soil evaporation (E) and canopy transpiration (T) under the assumption that the energy balance is closed. In most cases, the surface air available energy flux, net radiation (R_n), soil enthalpy flux (G), and changes in biomass energy storage (S) can be balanced against vertical turbulent fluxes of sensible (H) and latent (λET) enthalpy. The term S includes biomass enthalpy storage and metabolic or biochemical energy storage (Gu et al., 2007). A positive value of S indicates an increase in the amount of energy stored in the ecosystem. For ecosystems with tall trees (>8 m), the magnitude of S can be important (~5% of R_n) during short (e.g., 30 min) time intervals but is generally negligible (<5% of R_n) when integrated over timescales of a day or longer (Gu et al., 2007; Haverd et al., 2007). In this study, tree height only exceeds 8 m at the LZ site, suggesting that the S term may be significant there. However, lacking the necessary measurements to estimate this term, we have neglected it in the analysis. Furthermore, the flux G of enthalpy into the soil at any moment in time is only measured at the reference depth some time later owing to the time required for the enthalpy flux to reach the reference depth from the soil surface. This means that there is generally a time lag in G relative to the atmospheric fluxes. The time lag between the soil surface and the subsurface influences the accuracy of short-term (less than 6 hr) energy balance calculations in mangrove ecosystems, as evidenced by better energy balance closure at daily timescales relative to half-hourly timescales (Barr, Fuentes, et al., 2013). We have checked the monthly average diurnal cycle of energy exchange in the three mangrove ecosystems (Figure S3). For YX during 2011–2012, G lags R_n by 5 hr (10 * 30 min) in spring and winter and by 2.5 hr in summer and autumn, similar to the lags reported by Barr, Fuentes, et al. (2013). For LZ during 2015–2016, the lag time is 1.5 hr in all months, while for GQ during 2015–2016, the lag time is 1.5 hr in summer and autumn and 2.5 hr in winter and spring. Time series of G values were adjusted according to these characteristic lag times for each site and season.

Moreover, in mangrove ecosystems, tidal activity affects the energy balance via the exchange of enthalpy between the tidal water column and the air above or soil surface below (Barr, Fuentes, et al., 2013). We therefore have added a term representing enthalpy transfer into the tidal water column (G_w, see section 3.3) to the standard energy balance equation:

$$R_n - G - G_w = \lambda ET + H. \tag{7}$$

Conservation of energy requires that the left- and right-hand sides of this formula be equal. The slope of the least-squares regression line of the two sides can therefore provide an aggregate estimate of average surface energy budget closure. These slopes indicate 63% energy balance closure at GQ, 70% at LZ, and 72% at YX, indicating imbalances on the upper end of the range suggested by previous studies (10% to 30%; Wilson et al., 2002; Foken, 2008).

As the extent of energy balance closure determines the accuracy of energy available for further allocation into the soil surface and plant canopy, we take the following steps to reduce energy imbalances in the measured data. First, for 30-min periods under tidal inundation with values of $(\lambda ET + H)/(R_n - G - G_w)$ between 60% and 80%, we set the sum $G + G_w$ to $0.2 R_n$. This adjustment was motivated by the expectation of large errors in soil heat flux observations when the soil surface is covered by tidal water (Mezbahuddin et al., 2016) and guided by sensitivity tests in the energy balance response to variations of x in the $x R_n$ term (see detailed discussion below). Although the adjusted data account for only 0.15% of data at YX, 0.58% at GQ, and 0.13% at LZ, this adjustment improves energy balance closure by 4%, 5%, and 1%, respectively: Energy balance closure for the three mangrove ecosystems increases to 66% at GQ, 76% at LZ, and 82% at YX (Figure S4). We then corrected all observed latent enthalpy fluxes (λET_c) to account for the remaining lack of closure in the energy balance using the Bowen ratio ($\beta = H/\lambda ET$) method (Twine et al., 2000): $\lambda ET_c = (R_n - G - G_w)/(1 + \beta)$. This method can result in λET_c values exceeding EC-derived λET by 10–30% around midday, when the surface energy budget based on observations is furthest from closure (Twine et al., 2000). Values of λET_c were used for further analysis, including comparison with modeled values, in place of EC-derived λET.

3.2. The Traditional Two-Source Model in Brief

The two-source model is normally based on allocations of available energy into energy fluxes associated with soil evaporation and canopy transpiration, respectively. The allocation is modulated by a set of
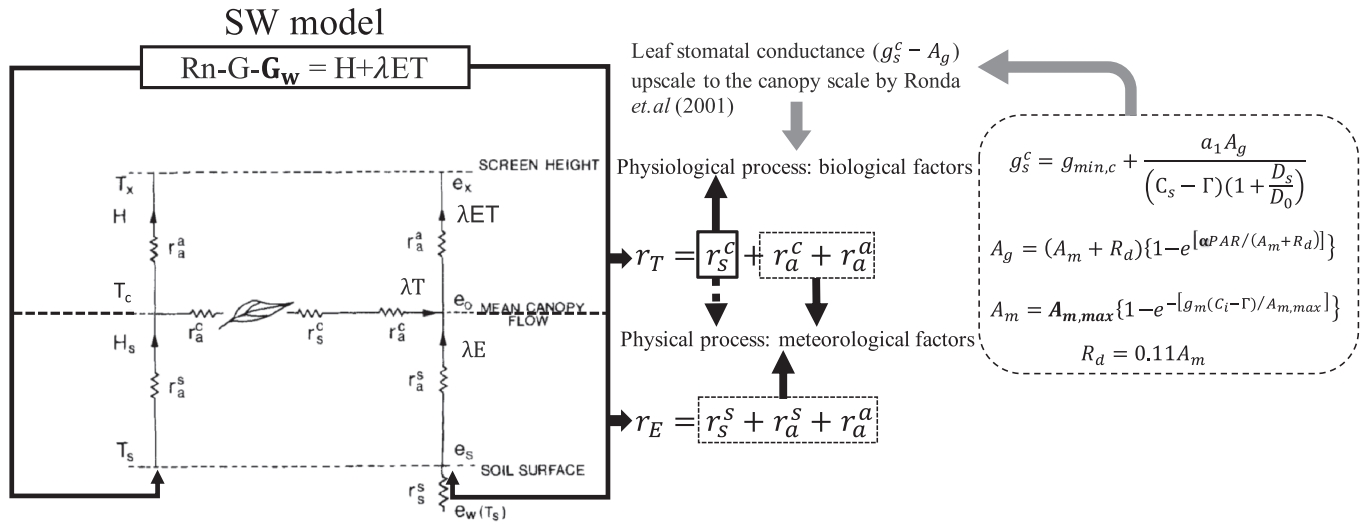
Figure 1. Schematic diagram of the two-source model for mangrove ecosystems, modified from Shuttleworth and Wallace (1985) and Ronda et al. (2001). Variables in bold indicate the aspects where we have modified this model, including G_w, α, and $A_{m,\max}$, as described in section 3.3. The parameters used in our formulation are listed in Appendix A. Other aspects of the model, including the detailed scheme for C_i (intercellular CO_2 concentration), follow Ronda et al. (2001).

resistances encountered by energy fluxes in series between the substrate surface and the reference height. The initial version of the two-source model, illustrated in Figure 1, was developed by Shuttleworth and Wallace (1985). They allocated available energy into sensible (H) and latent (λET) enthalpy fluxes, with the latter partitioned among soil evaporation and canopy transpiration according to the resistances encountered by each process (r_E and r_T). Ronda et al. (2001) modified the stomatal conductance-gross assimilation rate ($g_l^c - A_g$) module for estimating canopy resistance (r_s^c), as also illustrated in Figure 1. In their formulation, the gross assimilation rate (A_g) is a function of canopy temperature (T_{sk}), PAR, and the intercellular CO_2 concentration (C_i). The initial two-source model with default parameters for a flooded paddy field and adjustments only to parameters describing ecosystem conditions (such as heights for wind and temperature measurements, leaf size, and cuticular conductance for CO_2) was applied to YX mangrove forest. This model slightly overestimated the eddy-measured ET ($I = 0.94$, RMSE = 74.4) but significantly overestimated the sap flow-measured T ($I = 0.64$, RMSE = 111.7) in the YX mangrove forest (Table 2), especially around midday during summer.

Table 2
The Performance of the Two-Source Model in Simulating Canopy Transpiration (T) and Evapotranspiration (ET) Among Different Parameterization Schemes at the YX Site

Model type	Parameters		T		ET	
	Name	Value	I	RMSE (W m^{-2})	I	RMSE (W m^{-2})
Default (paddy field)	D_0	0.245	0.64	111.7	0.94	74.4
	G_w	0				
	S_w	0				
	T_1	281				
	T_2	311				
Modified	D_0	0.15	0.84	53.2	0.96	52.8
Modified1	G_w	Equation (8)	0.87	48.4	0.97	47.4
Modified2	S_w	Equation (9)	0.87	42.3	0.97	46.5
Modified3	T_1	290	0.94	34	0.98	46.0
	T_2	305				

Note. The modified steps are numbered sequentially; for example, Modified2 is conducted after Modified1, D_0 is a tunable value of vapor pressure deficit, and T_1 and T_2 are the lower and upper reference temperatures, respectively (equation (10)).

3.3. Adjustments to the Two-Source Model for Mangrove Ecosystems

To adapt the two-source model for use in mangrove ecosystems, we must further modify the initial model. Considering that stomatal conductance is relatively sensitive to large vapor pressure deficit (*VPD*) values, which often occur around midday during summer for mangrove trees (Krauss & Duberstein, 2010; Barr et al., 2014; Krauss, Barr, et al., 2015, Krauss, Duberstein, et al., 2015; Si et al., 2017), we first reduced the tunable parameter D_0 in equation (C1) from 0.245 (the default paddy value) to 0.15. The regression relationship between simulated and observed *ET* after these modifications yields $I = 0.96$ and RMSE = 52.8, with a more dramatic improvement in the relationship between simulated and observed *T* ($I = 0.84$ and RMSE = 53.2). Further adjustments to D_0 yield no further improvements in modeled *T* relative to observations. Therefore, more detailed modifications are needed. Considering the potential effects of high temperatures (especially during summer), tidal energy exchange, and salinity on evapotranspiration and its components, further modifications focus on representations of these three aspects in the two-source model.

First, one of the most important differences between mangrove ecosystems and fully terrestrial ecosystems is the impact of tidal fluctuations, as enthalpy exchange with tidal waters (G_w) may affect closure of the surface energy balance as indicated by equation (7) (Sobrado, 2007; Barr, Fuentes, et al., 2013). Allen et al. (2017) and Shoemaker et al. (2005) also found that the contributions of vertical exchange with surface water were an essential component of the surface energy budget in wetlands, particularly on dry winter days when surface energy exchanges were seasonally weak. Contributions of tidal water (G_w) to the surface energy budget consist of (1) vertical exchange between the tidal water and the air above or soil below (i.e., the net heating of surface water) and (2) lateral transport during ebb-and-flood tides (G_{adv}). We lack the necessary measurements to estimate G_{adv}; however, Barr, Fuentes, et al. (2013) showed that values of G_{adv} were close to zero during 12:00–16:00 in a mangrove ecosystem in Everglades National Park, United States. We therefore proceed under the limiting-case assumption that G_{adv} is negligible at all sites and only calculate the net heating of surface water. The value of G_w is then estimated as a function of water depth and water temperature (Heilman et al., 2000; Shoemaker et al., 2005):

$$G_w = C_w \times \rho_w \times \frac{h_w[i] + h_w[i-1]}{2} \times \frac{T_w[i] - T_w[i-1]}{1,800},$$ (8)

where C_w is the specific heat capacity of liquid water ($\approx 4{,}184 \text{ J kg}^{-1} \text{ K}^{-1}$), ρ_w is the density of water ($\approx 1{,}000 \text{ kg m}^{-3}$), h_w represents the water inundation depth, and T_w represents the average water temperature. The last two variables are estimated as vertical and temporal averages at each site during the ith 30-min time period, including only those measurements when the thermocouples were submerged. Theoretically, the water depth averaged over the whole drainage area should be equal to the ratio of water volume to drainage area, whereas we only have point measurements of water depth at each mangrove forest. These point measurements could still capture the main information on variations in tidal water depths (Lu, 2013); therefore, we approximate the average water inundation depth as $(h[i] + h[i-1])/2$ for the interval between the ith and $(i-1)^{\text{th}}$ time steps.

Second, mangrove plants, as halophytes, may have evolved unique tolerances to salinity that reduce the sensitivity of transpiration to salinity. However, the species dependence of these tolerances remains unclear. These uncertainties complicate efforts to quantify the effects of salinity on material and energy fluxes in mangrove ecosystems. With respect to water fluxes, the emerging consensus is that mangroves conserve water by reducing transpiration when salinities are high (Alongi, 2009; Krauss et al., 2006; Krauss et al., 2007; Lovelock & Ball, 2002). Recent research has also argued that photoinhibition levels in mangroves depend on environmental salinity (Barr et al., 2014; Barr, Engel, et al., 2013; Krauss et al., 2008; Lopez-Hoffman et al., 2007). LUE, as a key parameter in the $g_l^c - A_g$ canopy conductance module, may decrease as the salinity of tidal waters increases (Barr, Engel, et al., 2013; Cui et al., 2018; Krauss et al., 2008; Liu, 2015). Following the results reported by Barr, Engel, et al. (2013) for a mangrove ecosystem in Everglades National Park, we account for salinity effects on LUE by adding a term $0.014 \times S_w$ into the formula used by Jacobs (1994) and Ronda et al. (2001):

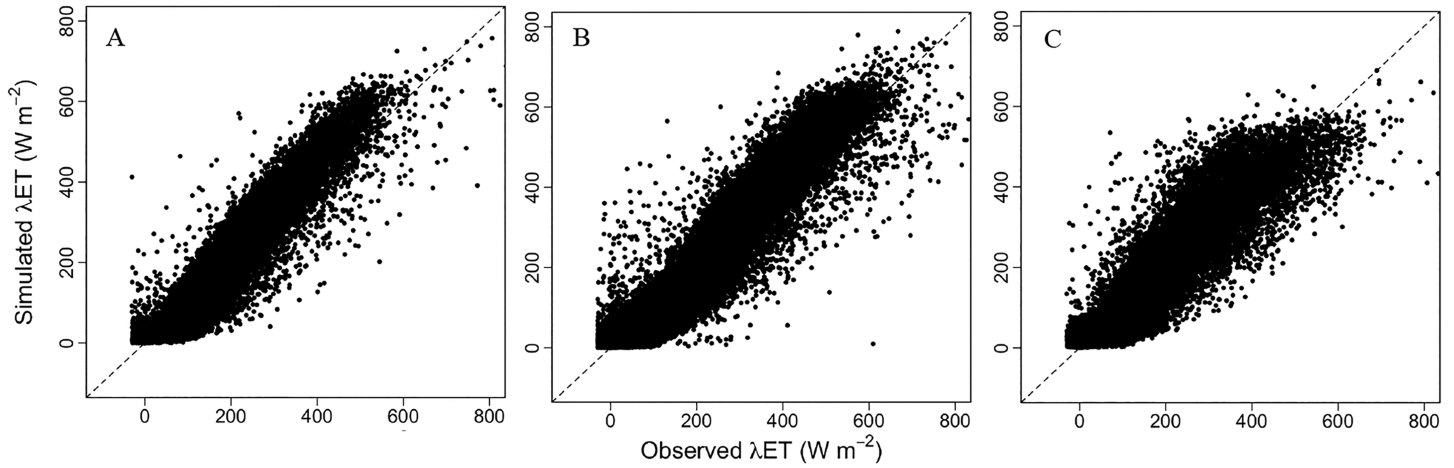$$\alpha = \alpha_0 \times \left(\frac{C_s - \Gamma}{C_s + 2\Gamma} \right) (1 - 0.0146 \times S_w).$$ (9)

Figure 2. Comparisons of half-hour evapotranspiration latent enthalpy fluxes (λET) simulated by the modified two-source model and observed by eddy covariance in three mangrove ecosystems: (a) YX, (b) GQ, and (c) LZ. The metrics of index of agreement (I) and root-mean-square error (RMSE) are $I = 0.98$ and RMSE = 46.0 W m^{-2} for panel a; $I = 0.98$ and RMSE = 41.7 W m^{-2} for panel b; and $I = 0.95$ and RMSE = 60.8 W m^{-2} for panel c.

Here, α represents LUE, α_0 is a reference LUE at low light conditions, C_s is the CO_2 concentration at the leaf surface, Γ is the CO_2 compensation point, and S_w is the salinity of the tidal water. Although some studies have suggested that salinity also affects stomatal conductance (Lin & Sternberg, 1992; Parida et al., 2004; Reef & Lovelock, 2015; Sobrado, 2000; Sobrado, 2005), the species dependence of these effects makes it difficult to draw consistent conclusions. However, variations in LUE ultimately alter canopy conductance (g_s^c) in the two-source model (see Appendix C), allowing us to assess whether the response of g_s^c to salinity in the model is reasonable (section 5.1.2).

Third, mangrove plants grow in an environment where temperatures and humidities are high year-round. These plants may therefore evolve special tolerances or sensitivities to these conditions (Ball et al., 1988; von Caemmerer & Evans, 2015). In light of these possibilities, we alter the temperature response curve in the plant physiology module:

$$Am, \max = \frac{X(T_{sk} = 298 \text{ K})Q_{10}^{(T_{sk}-298 \text{ K})/10}}{\left(1 + e^{0.3(T_1 - T_{sk})}\right)\left(1 + e^{0.3(T_{sk} - T_2)}\right)}, \tag{10}$$

where $A_{m,\max}$ denotes maximum primary productivity assuming abundant light and large CO_2 concentrations, T_{sk} is the leaf surface skin temperature (in Kelvins), and T_1 and T_2 are lower and upper reference temperatures used to adjust the temperature response of X to better match the results of field experiments (see section 5.1.3). The parameters used in our two-source model for mangrove ecosystems are listed in Appendix A. Further details regarding the two-source model structure and its mathematical formulation are presented in Appendices B and C.

4. Results

4.1. Performance of the Modified Two-Source Model

Values of ET simulated by the two-source model correlate well with EC estimates at all three mangrove sites after modifying the temperature response curve, accounting for the effects of salinity on light use efficiency, and including energy exchange with tidal water (Figure 2; for YX, GQ, and LZ, respectively: $I = 0.98$, 0.98, and 0.95 and RMSE = 41.7, 46.0, and 63.6 W m^{-2}).

The modified version of the two-source model also simulates variations in canopy transpiration fluxes in mangrove ecosystems well relative to sap flow-based measurements on both half-hourly and longer timescales (Figures 3 and 4). To account for time lags in the relationship between sap fluxes and canopy water vapor fluxes (Kume et al., 2008), sap flow data are compared with simulations of canopy transpiration fluxes 1 hr later in time. The high value of the index of agreement ($I = 0.95$, RMSE = 32.9 W m^{-2}) between modeled
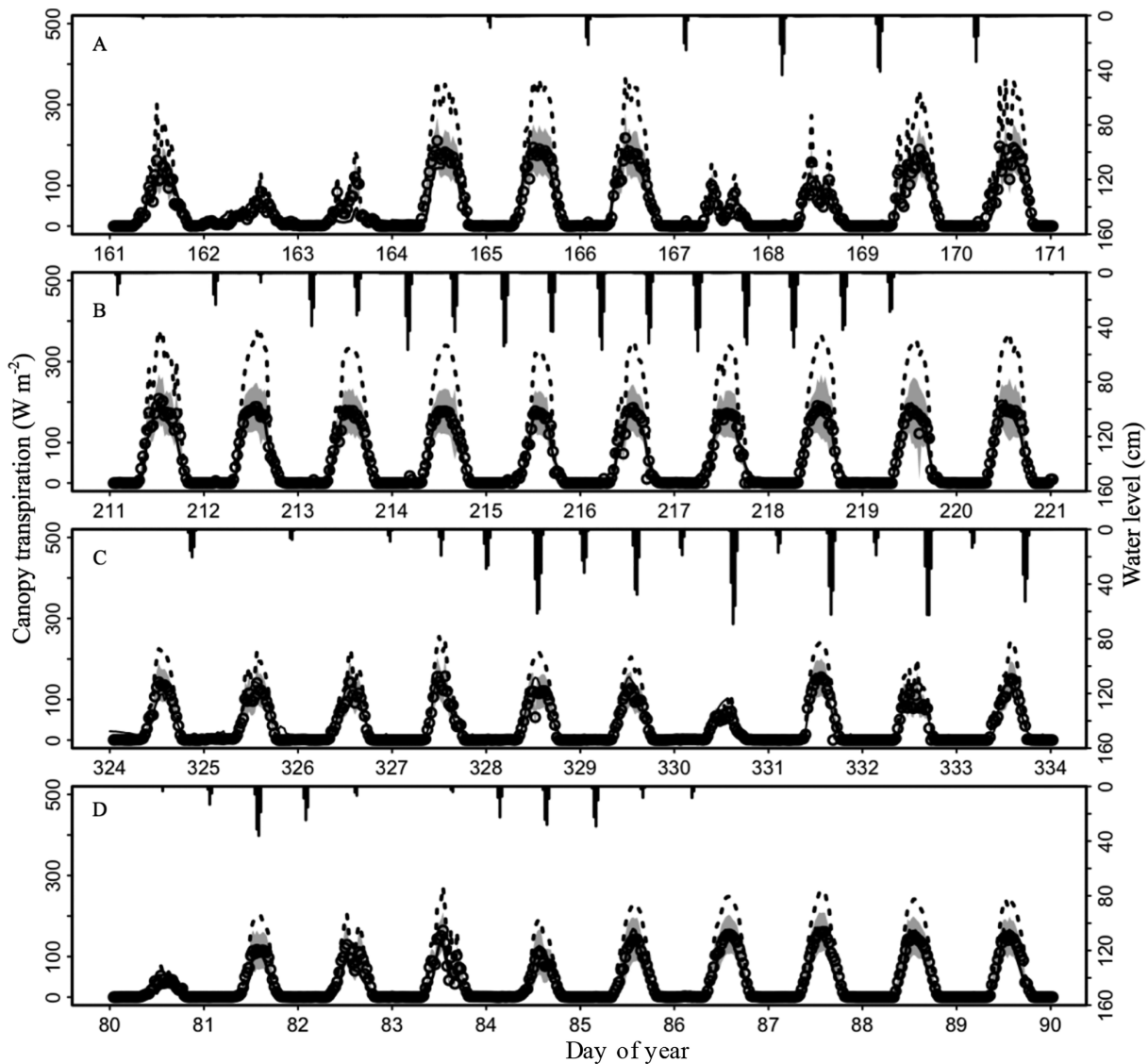
Figure 3. Canopy transpiration latent enthalpy fluxes measured via the sap flow technique (black line) and simulated by the modified two-source model (open circles) 10 typical days in (a) spring 2011, (b) summer 2011, (c) autumn 2011, and (d) winter 2012 at YX. Simulations based on the traditional two-source model with parameters used in a paddy field (dash line) are also included for context. An hour lag is applied to sap flow-based transpiration values relative to simulated canopy transpiration. The right *y* axis indicates water level during tidal inundation, shown along the top axis of each panel. Shading shows uncertainty in the simulations using the modified two-source model based on a Monte Carlo approach (500 times repeated random sampling from a normal distribution with parameter standard deviations equal to 10% of the original value).

and sap flow-measured canopy transpiration (T) marks the successful simulation of T in YX mangrove ecosystem based on upscaling stomatal conduction at leaf scales. However, the ratios of simulated T over simulated ET are less consistent with ratios based on observed values of ET and T (Figure 4b; $I = 0.63$, RMSE = 0.17). The simulated half-hourly T/ET ratios capture most of the variability in T/ET but with slight overestimates at smaller T/ET values and slight underestimates at larger T/ET values. The largest biases in both directions are associated with ET enthalpy fluxes less than 150 W m^{-2}.

4.2. Seasonality of *ET* and *T*

Measurements in all three mangrove ecosystems showed similar seasonal cycles of ET. In summer, when air temperature, evaporative demand (as represented by VPD), and LAI approached their annual maxima and salinity was relatively low (Figure S1), ET fluxes in the mangrove forests reached 8.3 ± 2.1 mm day^{-1} (mean $\pm$ standard error) at YX, 6.0 ± 1.4 mm day^{-1} at GQ, and 6.4 ± 0.3 mm day^{-1} at LZ (Figure 5). In contrast, in
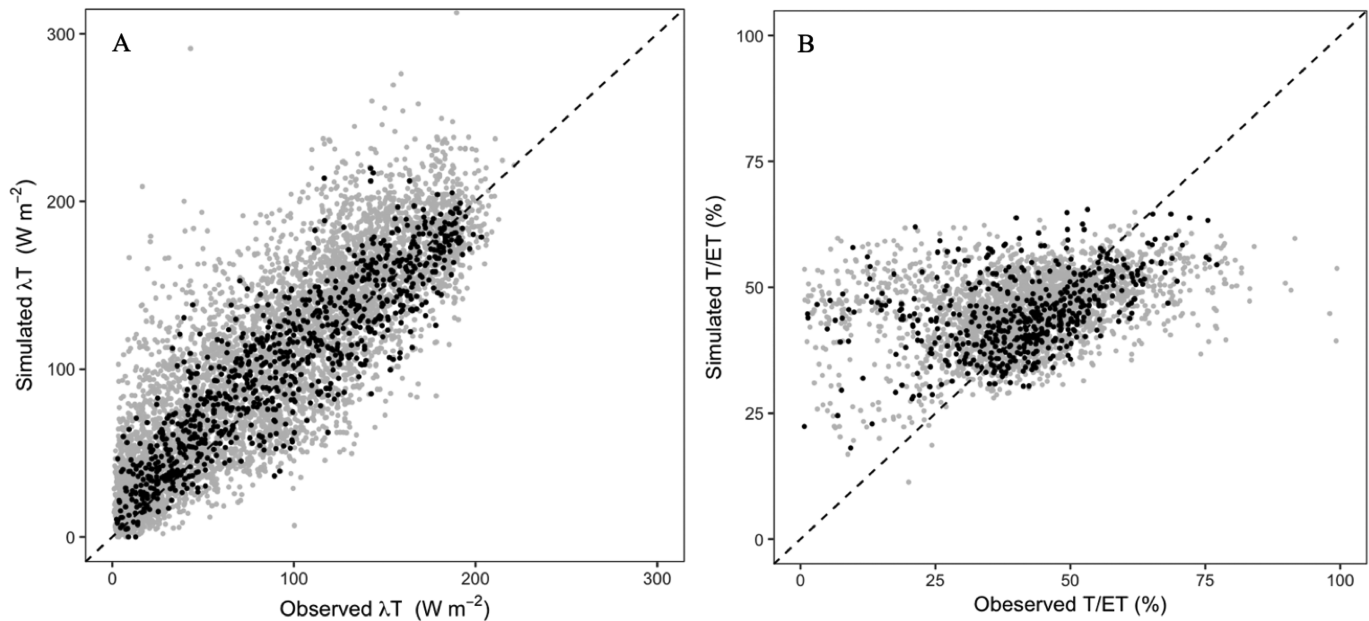
Figure 4. Comparisons of (a) canopy transpiration latent enthalpy fluxes (λT) between simulations using the modified two-source model and observations using the sap flow technique and (b) observed daytime T/ET based on sap flow-measured T and Bowen ratio-corrected ET and corresponding simulations (grey dots: all observed data; black dots: the data shown in Figure 3). For panel a, I = 0.95 and 0.97 and RMSE = 27 and 23 W m^{-2} for the grey and black points, respectively. For panel b, I = 0.63 and 0.65 and RMSE = 18.5% and 14.4%. The sap flow-measured half-hourly T values were filtered by conditions of relative humidity <0.8 and 150 W m^{-2} < net radiation. A 1-hr lag is applied to sap flow-based transpiration values before comparison against simulated canopy transpiration.

winter, when temperature and VPD were relatively low, ET fluxes in mangrove ecosystems were reduced to 2.2 ± 0.9 mm day^{-1} at YX, 2.5 ± 0.6 mm day^{-1} at GQ, and 3 ± 0.2 mm day^{-1} at LZ. Among the three sites, ET values during summer were lowest at YX, consistent with lower surface air temperatures and smaller evaporative demands at this site (Figures S1 and 5). Canopy transpiration fluxes inferred from sap flow measurements exhibited a similar seasonal cycle to that in ET, with average values of 1.3 mm day^{-1} at YX during winter rising to 2.5 mm day^{-1} during summer (Figure 3).

By contrast, contributions of T to ET (i.e., T/ET ratios) were smaller during summer than during autumn or spring (Figure S5). The observations indicate that T/ET ratios in autumn were $41.7 \pm 4.2\%$ at YX, significantly larger than summertime ratios of $34.8 \pm 1.0\%$.

5. Discussion

5.1. Factors Controlling Transpiration in Mangrove Ecosystems

Despite the abundance of surface waters in mangrove ecosystems, transpiration fluxes for mangrove trees are evidently constrained by stresses associated with high temperatures (e.g., Figure 3) and tidal fluctuations (e.g., days 328 through 330 in Figure S8). To clarify the effects of high temperatures and tides on T, we used the modified two-source model to probe potential response mechanisms and the special water relationships characteristic of mangrove ecosystems.

5.1.1. Tidal Effects

Contributions of tidal water to the surface energy budget (G_w) have been estimated to have monthly average magnitudes of −40 to +20 W m^{-2} via equation (8) (Figure S9), accounting for 2–5% of available energy. As a whole, the cumulative annual sums of half-hourly G_w at YX were negative, indicating a net release of stored tidal water heat energy to the mangrove ecosystem, while cumulative values at the GQ and LZ mangrove ecosystems were positive. The main difference in G_w terms between the GQ and YX ecosystems happened in autumn and winter when values of G_w were largest but other components of the surface energy budget were relatively small, consistent with the observations of Allen et al. (2017) and Shoemaker et al. (2005). Our addition of G_w into equation (7) improved energy balance closure in the three mangrove ecosystems
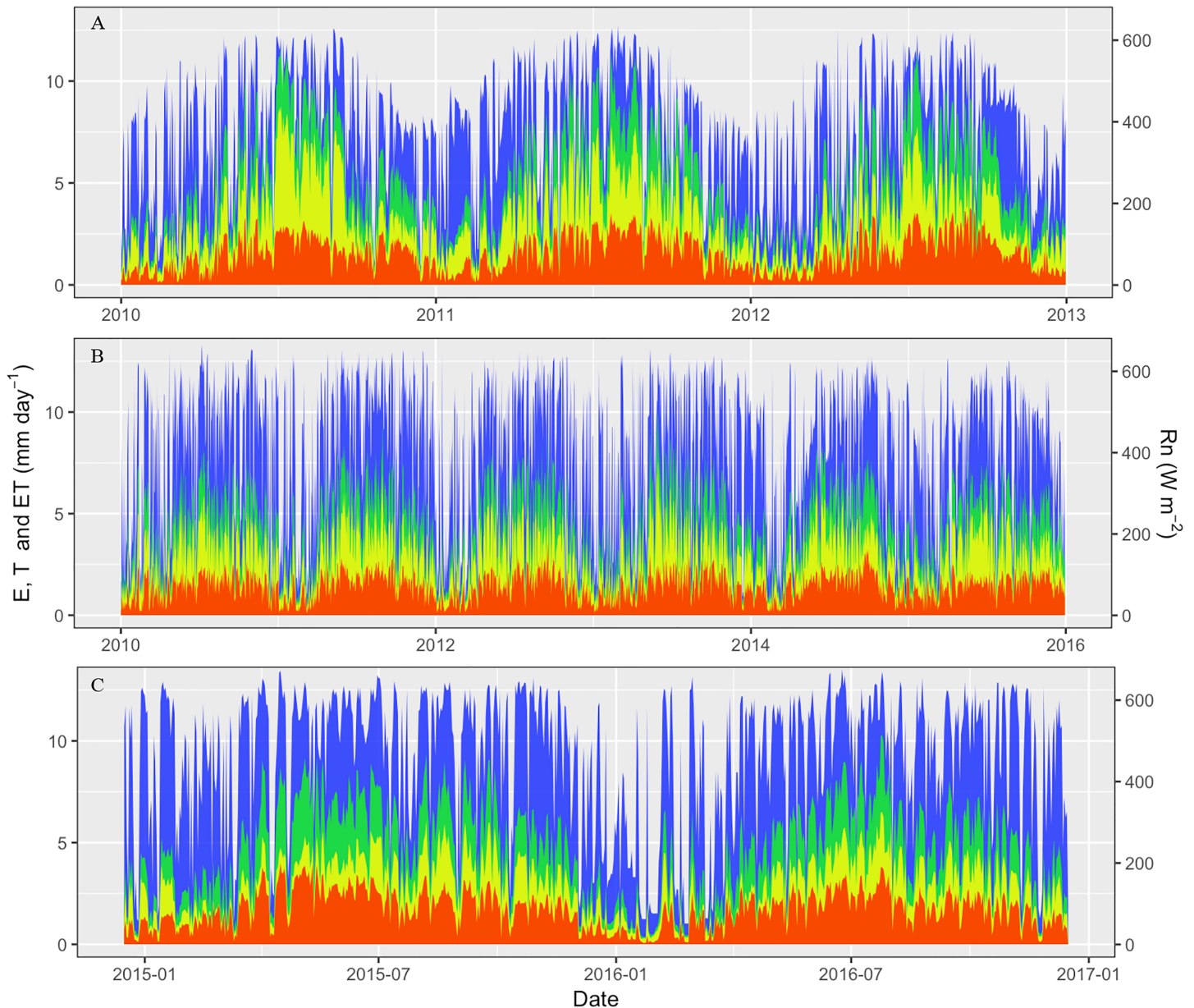
Figure 5. Seasonal dynamics of observed daily net radiation flux (blue), simulated evapotranspiration flux (green), canopy transpiration (red), and evaporation (yellow) by the modified two-source model at (a) YX, (b) GQ, and (c) LZ.

by 2% to 3%. Moreover, the index of agreement for *ET* increased by about 3% and that for *T* by about 1% in YX mangrove forest (Table 2).

Here, we also provide further explanation for setting half-hourly values of $G + G_w$ to $0.2R_n$ when the measurement sites are under tidal inundation and values of $(LE + H)/(R_n - G - G_w)$ are between 60% and 80%. Measurements of G based on the equipment used at these sites are subject to large errors when tidal water covers the soil surface (Mezbahuddin et al., 2016). We therefore consider adjusting the total changes in energy storage for soil and tidewater $(G + G_w)$ to obey the constraint $G + G_w = xR_n$ when energy budget closure is more than 60% but less than 80%. We have evaluated the response of the energy balance to a range of values for x (the coefficient by which R_n is multiplied) between 0.05 and 0.4 in increments of 0.05. We have selected 0.2 as the optimal coefficient based on the resulting values of the linear regression slope, R^2, and RMSE for energy balance closure during tidally inundated periods (Table S2).

Table 3

Sensitivity Tests of Daytime Half-Hour ET, T, and T/ET in Response to our Adjusted Parameters (Water Salinity [S_w], Water Temperature [T_w], and Depth [h_w]) and Some Main Input Variables (VPD and LAI)

	ET			T			T/ET		
Variable	YX	GQ	LZ	YX	GQ	LZ	YX	GQ	LZ
R_n	1.3	0.6	0.5	0.7	0.9	0.2	−1.0	−0.9	0.7
H	0.3	−0.4	−0.4	0.4	0.01	−0.1	−0.4	0.03	1.2
G	0.4	−0.3	−0.3	0.4	0.01	−0.1	−0.5	0.01	1.2
T_a	0.7	−0.1	−0.1	0.3	−0.3	−0.4	−1.0	−0.7	0.6
VPD	0.5	−0.3	−0.4	0.5	0.2	0.03	−0.5	0.3	1.2
LAI	0.5	−0.1	0.01	1.2	0.7	0.6	0.01	0.4	1.6
S_w	0.3	−0.3	−0.3	0.4	0.3	−0.2	−0.4	0.2	1.1
T_w	0.4	−0.4	−0.4	0.4	−0.01	−0.1	−0.5	0.01	1.2
h_w	0.4	−0.4	−0.4	0.4	−0.01	−0.1	−0.5	0.01	1.2

Note. SC is the sensitivity coefficient calculated for increments of ±0.1 via equation (6), where a value of 0.1 means a variation of 1% in the input variable is associated with a variation of 0.1% in the output variable. Daytime is 8:00–18:00 in this study.

Sensitivity tests based on YX data showed that water temperature and water depth, the two determinant factors of G_w, both had significant positive effects on ET and T (SC = 0.4 and 0.4, respectively) but negative effects (SC = −0.5) on T/ET in the modified model (Table 3). This suggest that a sea level rise of 1% or a water temperature (in °C) increase of 1% at YX would lead to a 0.5% reduction in T/ET. However, this situation likely does not apply at GQ and LZ (Table 3), where the cumulative annual values of G_w were positive. Our results thus imply that sea level rise or seawater warming (assuming fixed salinity) would cause different responses in water or carbon fluxes in different mangrove ecosystems.

5.1.2. Salinity Effects

For the YX mangrove forest, adapting the LUE response function to include a salinity dependence (equation (9)) slightly reduces the RMSE (Table 2) but does not significantly improve the performance of the two-source model in simulating canopy transpiration, presumably because salinity is relatively low at this site (0 to 24 PSU, Figure S1D). However, sensitivity tests on simulated T indicate that the low-salinity mangrove forests (YX and GQ) have opposite sensitivities to changes in salinity relative to the high-salinity LZ mangrove forest (Table 3), suggesting that low salinity is favorable to T while high salinity suppresses T. To further clarify the effects of salinity on canopy transpiration, we have conducted a wider model-based sensitivity test for the YX site, in which we increase the observed salinity in 20% increments from 0% to +60%. The results show slight increases in T as salinity increases from 0 to 15 PSU, indicating salt tolerance, but significant decreases in T with increasing salinity when salinity exceeds 28 PSU (Figure 6).

Moreover, this modification significantly altered simulated stomatal conductance (Figure 7b; R^2 = 0.20, P < 0.001) at the LZ site, where the range of salinities was larger (0 to 54 PSU) relative to the other two sites. Model results and observations consistently suggest that salinity-based inhibition of stomatal conductance becomes influential at salinities greater than 28 PSU (Figure 7). Previous studies have found that most mangrove species, as obligate halophytes (Wang et al., 2011), grow best in waters with salinities around 15 PSU, with distinct differences in stomatal behaviors when salinity exceeds 28 to 30 PSU (Biber, 2006; Clough & Sim, 1989; Lloyd et al., 1987; Lovelock & Ball, 2002; Reef et al., 2012; Reef & Lovelock, 2015). Our modified model also suggests significant suppression of H_2O stomatal conductance (g_l^c) when salinity exceeds 28 PSU and R_n exceeds 300 W m^{-2} (i.e., when effects of radiation on g_l^c are largely eliminated; Figure 7b). Data from previously published field studies are in good agreement with our proposed model for variations in stomatal conductance with salinity (Figure 7).

5.1.3. Temperature Effects

The two-source model using default parameters for paddy fields overestimated observed canopy transpiration in these mangrove sites, especially at times when temperatures were high (at noon and in summer; Figure 3). We therefore hypothesize that water use by mangrove trees may be more conservative when temperatures are high (Quisthoudt et al., 2012). Previous studies have suggested that transpiration and carbon fluxes in mangroves maximize when leaf temperatures are between 300 and 303 K (Alongi, 2009; Barr et al., 2009; Boyd & Kohlmeyer, 1982). Further increases in temperature can cause partial stomatal closure, with photosynthetic enzyme inhibition at temperatures larger than 308 K (Ball et al., 1988; Ball & Farquhar, 1984; Buckley, 2005). The optimal temperatures for leaf carbon assimilation ($A_{m,\max}$) in the standard physiological module of the two-source model are set to 308 and 307 K respectively for C_3 plants (Ronda et al., 2001). Moreover, recent research has suggested a positive relationship between $A_{m,\max}$ and stomatal density (Tanaka et al., 2013). Mangroves have smaller stomatal density (Liang et al., 2018), which implies a smaller $A_{m,\max}$ relative to neighboring C_3 or C_4 plants. We have therefore adjusted the reference temperatures T_1 and T_2 in equation (10) to reduce both the optimal temperature value for $A_{m,\max}$ (to 303 K) and the peak value of $A_{m,\max}$ associated with that optimal temperature (Figure 8 and Table 2). In the resulting temperature response curve, $A_{m,\max}$ decreases to zero at 315 K (Cheeseman et al., 1997). This change in the temperature curve dramatically improves the performance of the two-source model with respect to simulating canopy transpiration in mangrove ecosystems, with improvements in simulated T of up to 17% relative to
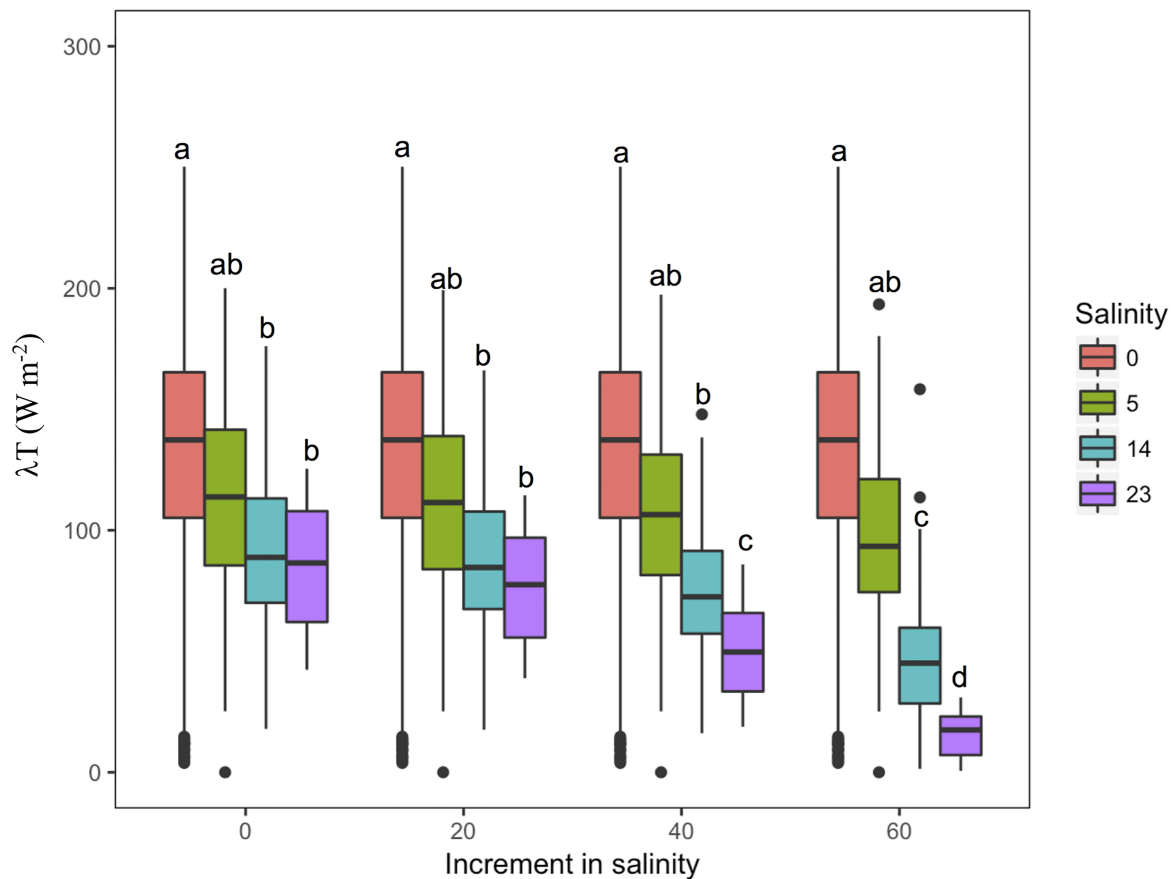
Figure 6. Sensitivity tests at YX mangrove focusing on how canopy transpiration fluxes respond to increasing salinity. Observed values of salinity in four groups (far left) are artificially augmented by 20% (center left), 40% (center right), and 60% (far right). The colors represent salinity groups with initial mean values of 0 (red), 5 (green; range 0–10), 14 (cyan; range 10–20), and 23 PSU (purple; range 20–30). Lowercase letters above each bar indicate when differences are significant at the 95% confidence level ($P < 0.05$) based on the Tukey "honest significant difference" test, ordered by decreasing magnitude along the y axis. Boxes encompass the 25th to 75th percentiles of each distribution, with the median marked by a horizontal line inside the box. Outer bars encompass the entire range excluding extreme outliers (values more than 1.5 times the interquartile range from the median). Extreme outliers are shown as black circles.

the default temperature schemes for C_3 plants (Table 2). This significant improvement supports our hypothesis that the sensitivity of photosynthesis to high temperatures is greater in mangrove ecosystems than in most fully terrestrial ecosystems. Sensitivity tests on simulated data for the three mangrove forests suggests that variations in ET and T are most sensitive to variations in air temperature that result from fluctuations in solar radiation (Table 3). In particular, negative values of the sensitivity coefficients at the GQ and LZ mangrove forests, where temperatures are typically higher than at YX, imply that extreme high temperature is a key limiting factor for T in mangrove ecosystems.

5.1.4. Attribution of Seasonal Variations in Tidally Influenced T

Based on data measured using the sap flow technique, we identify R_n, air temperature, and VPD as the main drivers of seasonal variations in transpiration (correlation coefficients: 0.9, 0.8, and 0.7, respectively). However, VPD contributed substantially only when both VPD and R_n were large (Figure S7A). The effect of R_n on T was reduced when air temperatures were large because canopy conductance is suppressed at high temperatures (Figure 9). Likewise, T and E had different responses to variations in VPD in mangrove ecosystems, with a weaker response in T than in E (Figures S7A and S7C). The response of T to variations in VPD was also weaker than that observed in other well-watered forest ecosystems (Ball, 1996; Krauss, Barr, et al., 2015; Muller et al., 2009; Oren et al., 1999), although responses of T to VPD were enhanced under flood tides (Figures S7B and S7D). Suppression of T (due to reduced stomatal conductance) and stimulation of E under high-temperature conditions result in a decrease of T/ET. These responses may then be further modulated by salinity effects (Figure 9).
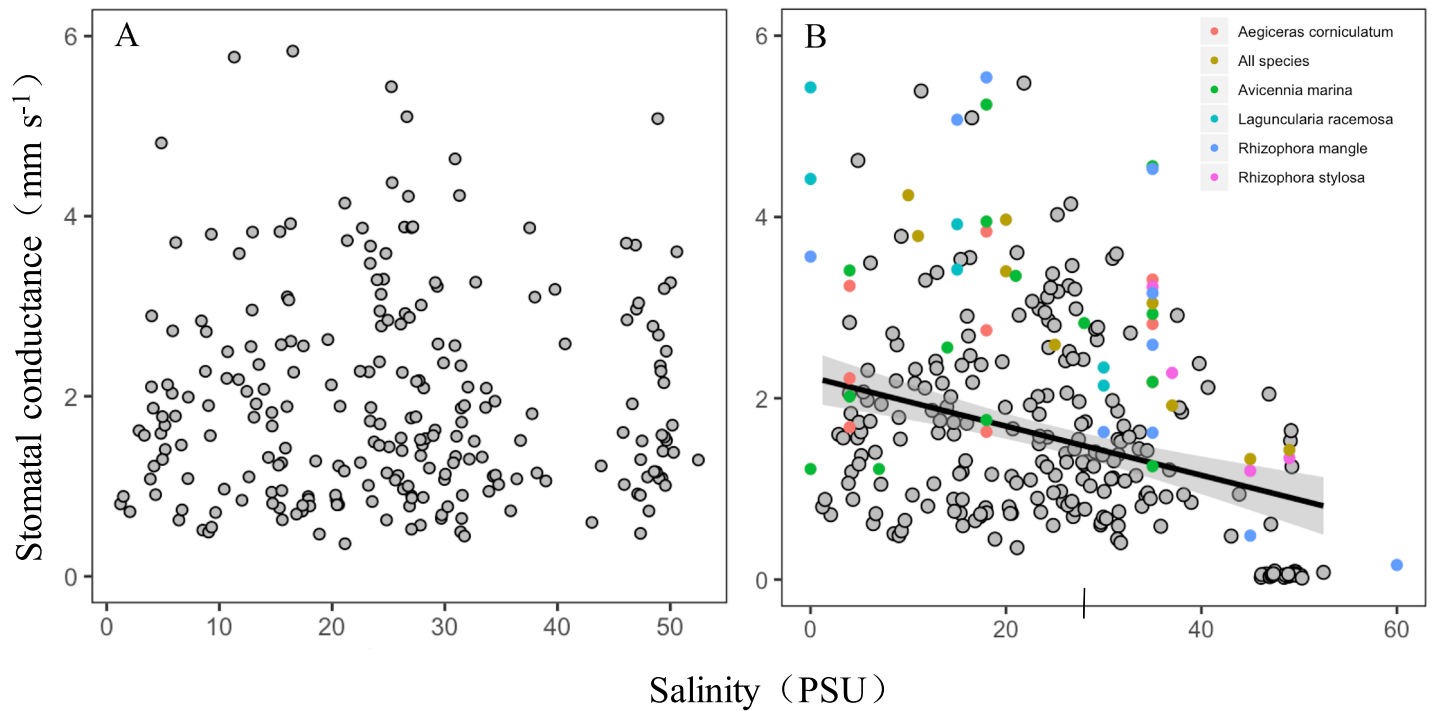
Figure 7. Relationship between half-hourly simulated stomatal conductance and salinity (unit: PSU) when net radiation exceeded 300 W m^{-2} at LZ under two scenarios: (a) without the salinity term and (b) with the salinity term in equation (9). In panel b, the black line indicates the linear fit to the data ($P < 0.05$), and the shading represents the 95% confidence interval in this linear fit. The black vertical line along the x axis in (b) marks 28 PSU. Colored points indicate measurements collected from previously published studies (Ball, 1988; Biber, 2006; Clough & Sim, 1989; Lin & Sternberg, 1992; Nguyen et al., 2015; Sobrado, 2005).
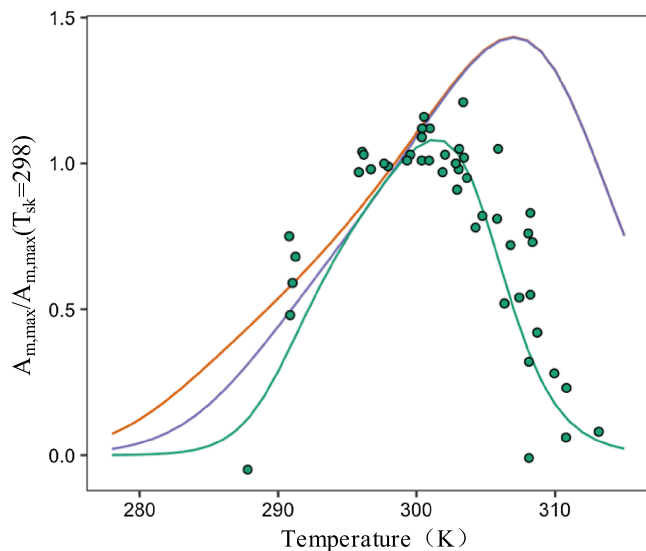

Figure 8. Comparison of variations of maximum photosynthesis rate ($X = A_{m,max}$ in equation (10)) per $A_{m,max}$ (T_{sk}=298) with leaf temperature (T_{sk}) among C_3 (red curve; $T_1 = 281$, $T_2 = 311$), C_4 (blue curve; $T_1 = 286$, $T_2 = 311$), and mangrove (darkgreen curve; $T_1 = 290$, $T_2 = 305$) plant types. The curves are regulated by setting the reference temperatures T_1 and T_2 in equation (10). Green dots represent observations in three mangrove species under three irradiation gradients by Ball et al. (1988).

5.2. Characteristics of Water Fluxes in Mangrove Ecosystems
5.2.1. Comparison of Water Fluxes Among Mangrove Ecosystems

Annual T values among six subtropical mangrove ecosystems (including the three examined in this work and three discussed in previously published work; Krauss, Barr, et al., 2015) vary between 350 and 870 mm year^{-1} (Table S3). Differences in T among mangrove communities reflect multiple environmental factors, including temperature, freshwater availability, nutrient availability, salinity, and tides. Among these factors, a clear relationship between tidal water salinity and T emerges only when salinity exceeds 28 PSU ($P = 0.07$, Figure 10a), consistent with the behavior of our modified two-source model. The effects of tidal regimes on water fluxes in mangrove ecosystems are also evident in ET, as ET was significantly larger in the YX mangrove forest than in the GQ mangrove forest despite air temperature being larger at GQ. This difference is driven in part by the net release of stored heat energy in surface water ($G_w < 0$) associated with wintertime tides at YX, in contrast to a net absorption ($0 < G_w$) at GQ (Figures S9A, S9B, and S6). T/ET also varied from 30% to 66% among mangrove communities, with values tightly correlated with LAI ($P < 0.01$, Figure 9b). A larger LAI results not only in less solar radiation reaching the soil surface but also in a larger canopy transpiration flux, thus leading to larger T/ET ratios. Ratios of ET to precipitation also vary substantially among ecosystems, with values ranging from 0.7 to 2.1; however, these values are all significantly larger than those associated with terrestrial ecosystems (Table S3), suggesting that water subsidies provided by rivers or seas are essential for these mangrove ecosystems.
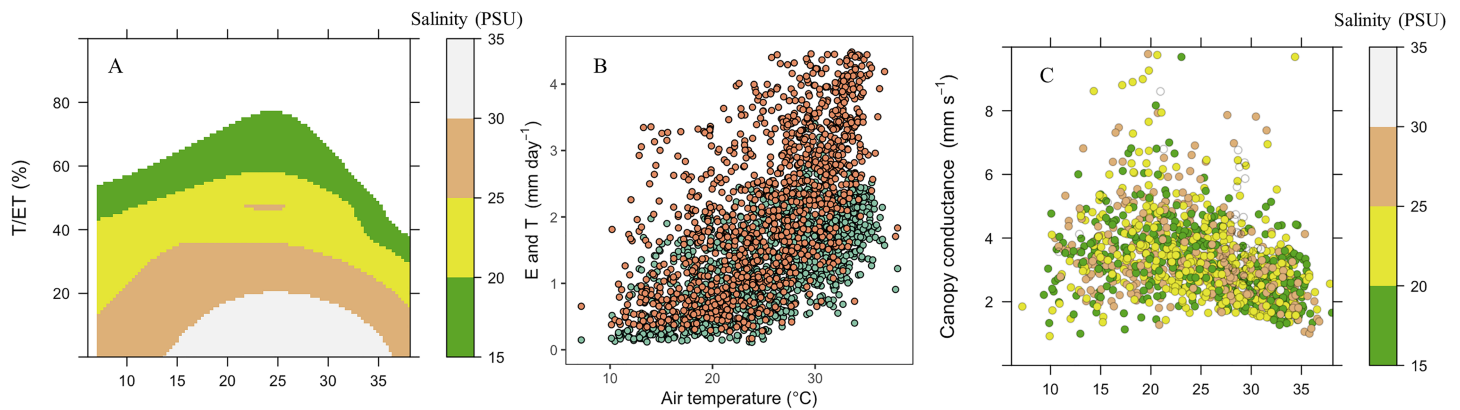
Figure 9. Relationships of the daily ratio of transpiration to evapotranspiration (*T*/*ET*, panel a), surface evaporation (*E*, orange in panel b), canopy transpiration (*T*, dark green in panel b), and canopy conductance (panel c) with daily air temperatures in three mangrove forests. Data of water fluxes at the YX mangrove forest are from observation, and those at the other two are from simulations. To better illustrate the interaction of salinity and temperature, panels a and c only show data in the 15–35 PSU salinity range.

5.2.2. Comparison of Water Fluxes in Mangrove Ecosystems and Fully Terrestrial Ecosystems

In contrast to close associations between *LAI* and canopy conductance on seasonal timescales in most terrestrial ecosystems, we find no evidence of significant links between these variables at the mangrove sites (correlations <0.2 at all three sites), although *T* has a similar seasonal pattern to *LAI* (Figures 5 and S1). This similarity emerges because both variables are linked to the same driving factor: air temperature. The difference between mangroves and other terrestrial ecosystems may arise in part because seasonal variations in *LAI* are smaller in mangrove ecosystems (Figure S1D) than in most terrestrial ecosystems (Berkelhammer et al., 2016; Wang et al., 2014; Wei et al., 2018). Plus, the more sensitive response of leaf stomatal conductance to environmental factors (such as temperature and salinity) may mask the effects of *LAI* on canopy conductance, in accordance with the equation for canopy conductance proposed by Ronda et al. (2001).

Unlike most terrestrial ecosystems, surface evaporation (*E*) dominates water fluxes between mangrove ecosystems and the ambient atmosphere above them. As *E* fluxes are driven primarily by meteorological factors, both *E* and *ET* vary in parallel with the seasonal cycles of solar radiation and evaporative demand at our study sites (Figures S1 and 6). During winter, *ET* fluxes in these mangrove forests are consistent with those in semiarid ecosystems (Choi et al., 2012; Wang et al., 2013). During summer, *ET* fluxes in these same mangrove forests are more consistent with those in well-watered broadleaf forests (Kunert et al., 2017; Shuttleworth, 1988; Tan et al., 2015; Xiao et al., 2013). Owing to abundant water availability for evaporation and intense solar radiation year-round, the annual *ET* in mangrove ecosystems (approximately 1,300 mm year^{-1}) is comparable to that observed in tropical rainforests (Table S3). However, *T* remains low throughout the year, especially in mangroves where surface water salinity is large (Figure 10b). Mangrove ecosystems with smaller salinities had annual *T* fluxes close to those in evergreen forests, while mangrove forests with larger salinities had annual *T* fluxes closer to those associated with arid and semiarid grasslands (Table S3).

The ratio of daily and monthly canopy transpiration to total evapotranspiration (*T*/*ET*; Figure S5) was likewise lower than the ratios observed in other types of tropical and subtropical forests (Wei et al., 2017). Moreover, observed seasonal variations in *T*/*ET* at the mangrove sites differed from those reported for most terrestrial ecosystems. Average *T*/*ET* ratios were lower during summer (30–38%) than during autumn (35–53%) at all three sites. We ascribe these atypical seasonal variations to two factors. First, high midday air temperatures during summer (Figure S1) suppress canopy conductance but not surface evaporation (Figure 9c), while air temperatures during autumn are more favorable for enhanced transpiration. Second, tidal inundation can suppress *T*/*ET* (Figures 9a and S8), either because salinity limits stomatal conductance or because the water supply (root function) is inhibited by low O$_2$ and high salinity (Ball, 1988, 1996, 2002). Lower salinity associated with relatively strong rainfall events during autumn should therefore act to increase the ratio of *T*/*ET* in these mangrove ecosystems relative to the summer months.
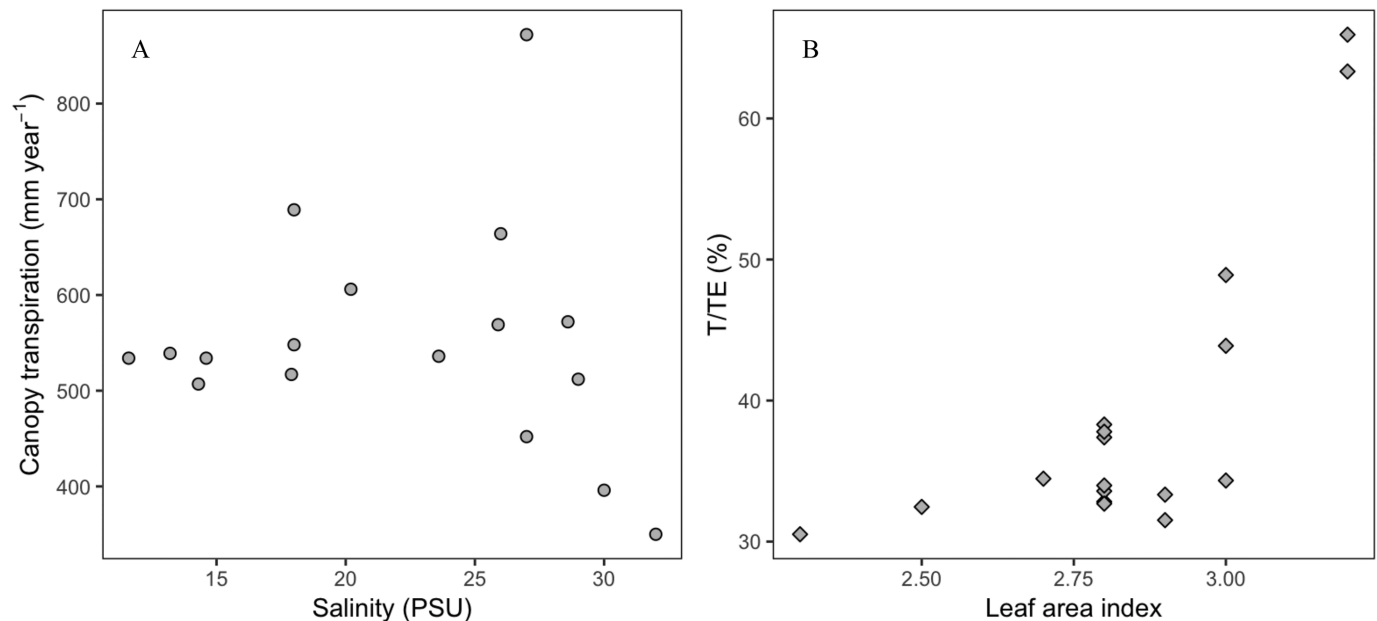
Figure 10. Relationships of (a) annual T and annual mean surface water salinity and (b) T/ET against LAI in six mangrove ecosystems. Data values are listed in Table S3 including our three mangrove ecosystems in China and three from Krauss, Barr, et al. (2015) in the United States.

5.2.3. Uncertainties in Estimated ET, T, and T/ET

The simulated results are affected by uncertainties in the assumptions involved in our method as well as by uncertainties in key input parameters. The former is difficult to avoid in most mathematical models and has been discussed above. Here, we only discuss the latter (uncertainties in key input parameters), which could potentially be reduced by more accurate measurements. Our sensitivity tests suggest that variations in ET, T, and T/ET are most sensitive to changes in net radiation and air temperature (Table 3). We therefore focus on evaluating the scale of uncertainties in T associated with air temperature. A Monte Carlo analysis suggests that uncertainties in half-hourly estimates of T were larger under higher temperatures than under lower temperatures (Figure 3). LAI also exerts significant impacts on simulated variations in transpiration fluxes, particularly at the YX mangrove forest, suggesting that accurate measurements of LAI in mangrove forests are important to the reliability of simulated T.

Moreover, the simulated T, ET, and T/ET are all sensitive to variations in the temperature, depth, and salinity of tidal water (Table 3). Therefore, accurate measurements of tidal properties are another prerequisite for reliable model performance under fluctuating tides. However, our single-site measurements of tidal variability in each mangrove ecosystem can only crudely represent the actual tidal regimes. Only one tide gauge was installed in each mangrove forest, and these single-site observations record tidewater conditions only at the gauge location. Lu (2013) confirmed that our measurements of tidal fluctuations at the YX and GQ sites capture most aspects of the associated tidal regimes, but more complete information on the structure of tidal creeks and actual measurements of tidal properties at multiple sites along those creeks would undoubtedly improve the representation of tidal effects in this model.

Uncertainties in T/ET were consistently larger at smaller values of ET (Figure 4b), which can be partially ascribed to errors in EC ET measurements at low friction velocities (Foken, 2008; Wilson et al., 2002). After removing data with $u_* < 0.1$, the linear index of agreements between simulations and observations of T/ET increases from $I = 0.63$ to 0.67. Energy imbalances at lower values of ET might be another important reason. For example, the energy closure at the YX site is 0.99 for times when half-hourly ET values exceeded $150\,\mathrm{W\,m^{-2}}$, but 1.33 when all data are included. Energy fluxes in the two-source model are forced to balance using the Bowen ratio method, causing large errors at small values of ET and H that then propagate into the allocation of ET into E and T. Eliminating data points with $ET < 150\,\mathrm{W\,m^{-2}}$ reduces the RMSE from 34.4% to 24.4%. Moreover, potential vapor or fog water absorption by mangrove leaves under high relative humidity (>0.8) might suppress transpiration, an effect that is not represented in the simulations. These phenomena

have been observed in some coastal species (Burgess & Dawson, 2004; Limm et al., 2009), but their importance in mangroves remains unknown. When we restrict the data to relative humidity values less than 0.8, most of the model overestimates disappear and the RMSE is reduced by nearly half (from 24.4% to 14.4%). The large sample size helps to mask these adverse effects on the simulation of T and ET, but T/ET ratios are sensitive to even relatively small errors in the simulated water fluxes. As a result, simulations of T/ET ratios require more accurate input data, and more caution is required when using simulated values of T/ET as opposed to simulated values of T or ET.

6. Conclusions

We have examined observed and simulated variations of evapotranspiration and its subcomponents in three mangrove ecosystems located in southern China. The magnitude of summer evapotranspiration in these mangrove forests was similar to that in well-watered broadleaf forests, with average ET fluxes of 6.2 mm day^{-1}. These same mangrove forests produced winter ET fluxes more comparable to those of semiarid ecosystems, with average values of 2.6 mm day^{-1}. Meanwhile, canopy transpiration rates in the mangrove ecosystems were comparable to those of semiarid grassland ecosystems year-round, with average fluxes of 2.5 mm day^{-1} in summer and 1.3 mm day^{-1} during winter.

Relative to most terrestrial ecosystems, seasonal variations of T in mangroves are more strongly affected by high temperatures. Suppression of T via limitation of canopy conductance at high temperatures, combined with stimulation of E, results in lower values of T/ET in summer than in autumn. Responses to variations in tidal water properties, such as reduced salinity when precipitation is large, are superimposed on these temperature effects.

We propose a modified version of the two-source model that enables quantitative evaluation of perturbations in ET and T in mangrove ecosystems under high temperatures, tidal inundation, and surface water salinity. Canopy transpiration reflects not only ecosystem productivity but also the functioning of an ecosystem under water stress. Our model's ability to quantify these unique relationships in mangroves will therefore improve our understanding of how mangrove ecosystems may respond to current and future climate change, including sea level rise and increases in the frequency of extreme weather events.

Appendix A: The Two-Source Evapotranspiration Model

Appendix B: The Structure of the Shuttleworth and Wallace Two-Source Model

Based on Shuttleworth and Wallace (1985), the evapotranspiration (ET) is partitioned into canopy transpiration (T) and soil surface evaporation (E) as

$ET = T + E = \omega_c PM_c + \omega_s PM_s,$

(B1) where the PM terms are analogous to the Penman-Monteith combination equations and the subscripts s and c indicate the soil and canopy components, respectively. The equations have the form:

$$PM_c = \frac{\Delta A + \left(\rho C_P D - \Delta r_a^c A_s\right)/\left(r_a^a + r_a^c\right)}{\Delta + \gamma\left[1 + r_s^c/\left(r_a^a + r_a^c\right)\right]}, \tag{B2}$$

$$PM_s = \frac{\Delta A + \left(\rho C_P D - \Delta r_a^s (A - A_s)\right)/\left(r_a^a + r_a^s\right)}{\Delta + \gamma\left[1 + r_s^s/\left(r_a^a + r_a^s\right)\right]}, \tag{B3}$$

$$\omega_c = \frac{1}{1 + R_c R_a [R_s(R_c + R_a)]}, \tag{B4}$$

$$\omega_s = \frac{1}{1 + R_s R_a [R_c(R_s + R_a)]}, \tag{B5}$$

$$R_a = (\Delta + \gamma) r_a^s, \tag{B6}$$

$$R_s = (\Delta + \gamma) r_a^s + \gamma r_s^s, \tag{B7}$$

$$R_c = (\Delta + \gamma) r_a^c + \gamma r_s^c, \tag{B8}$$

Table A1
Nomenclature

Variables	Value	Unit	Description	Data source
A	Measured	$\mathrm{W\ m^{-2}}$	Total available energy	This study
A_g	Calculated	$\mathrm{mg\ m^{-2}\ s^{-1}}$	Gross assimilation rate	Ronda et al. (2001)
A_m	Calculated	$\mathrm{mg\ m^{-2}\ s^{-1}}$	Primary productivity	Ronda et al. (2001)
A_{m,max_298}	2.2	$\mathrm{mg\ m^{-2}\ s^{-1}}$	Maximal A_m under high light and large CO_2 concentrations at 298 K	Chen et al. (2008)
A_s	Calculated	$\mathrm{W\ m^{-2}}$	Available energy of the substrate level	Shuttleworth and Wallace (1985)
α_0	0.017	$\mathrm{mg\ J^{-1}}$	Initial (at low light conditions) light use efficiency	Ronda et al. (2001)
a_1	9.1	—	$1/1 - f_0$	Ronda et al. (2001)
C_d	0.2	—	Drag coefficient	Shuttleworth and Wallace (1985)
C_i	Calculated	$\mathrm{mg\ m^{-3}}$	Intercellular CO_2 concentration	Ronda et al. (2001)
C_l	Measured	$\mathrm{mg\ m^{-3}}$	CO_2 concentration at the leaf surface	This study
C_p	1,004	$\mathrm{J\ kg^{-1}\ K^{-1}}$	Specific heat of dry air at constant pressure	Shuttleworth and Wallace (1985)
D_0	0.15	kPa	A tunable empirical parameter	This study
d_0	Calculated	m	Zero-plane displacement	Choudhury and Monteith (1988)
D	Measured	kPa	Vapor pressure deficit	This study
d_l	Measured	m	Leaf dimension	This study
f_0	0.89	—	An empirical parameter	Ronda et al. (2001)
g_m	Calculated	$\mathrm{mm\ s^{-1}}$	Mesophyll conductance	Ronda et al. (2001)
$g_{\mathrm{min},c}^*$	0.06	$\mathrm{mm\ s^{-1}}$	Cuticular conductance for CO_2	Chen et al. (2008)
g_m_298	7	$\mathrm{mm\ s^{-1}}$	Mesophyll conductance for CO_2 at 298 K	Ronda et al. (2001)
g_l^c	Calculated	$\mathrm{mm\ s^{-1}}$	Stomatal conductance for CO_2	Ronda et al. (2001)
h_c	Measured	m	Vegetation high	This study
k_r	0.6	—	Canopy extinction coefficient of net radiation	Ross (1981)
k	0.4	—	Von Karman constant	Brutsaert (1982)
κ_m	2.5	—	Extinction coefficient of the eddy diffusion	Brutsaert (1982)
K_h	Calculated	—	Eddy diffusion coefficient at the top of the canopy	Brutsaert (1982)
$Q_{10}\_g_m$	2	—	Ratio of g_m at one temperature to that at temperature 10° lower	Ronda et al. (2001)
$Q_{10}\_A_{m,\mathrm{max}}$	2	—	Ratio of $A_{m,\mathrm{max}}$ at one temperature to that at temperature 10° lower	Ronda et al. (2001)
R_d	$0.11Am$	$\mathrm{mg\ m^{-2}\ s^{-1}}$	Dark respiration	Ronda et al. (2001)
R_{ns}	Calculated	$\mathrm{W\ m^{-2}}$	Net radiation reaching the substrate	Shuttleworth and Wallace (1985)
r_s^c	Calculated	$\mathrm{s\ m^{-1}}$	Canopy resistance	Ronda et al. (2001)
r_s^s	Calculated	$\mathrm{s\ m^{-1}}$	Soil surface resistance	Sellers et al. (1992)
r_a^c	Calculated	$\mathrm{s\ m^{-1}}$	Canopy boundary-layer resistance	Shuttleworth and Wallace (1985)
r_a^s	Calculated	$\mathrm{s\ m^{-1}}$	Soil boundary-layer resistance between the soil surface and the canopy layer	Shuttleworth and Wallace (1985)
r_a^a	Calculated	$\mathrm{s\ m^{-1}}$	Aerodynamic resistance between the canopy source and a reference height	Shuttleworth and Wallace (1985)
r_b	Calculated	$\mathrm{s\ m^{-1}}$	Mean boundary-layer resistance	Shuttleworth and Wallace (1985)
$T_1\_g_m$	278	K	Lower reference temperature for g_m	Ronda et al. (2001)
$T_1\_A_{m,\mathrm{max}}^*$	290	K	Lower reference temperature for $A_{m,\mathrm{max}}$	This study
$T_2\_A_{m,\mathrm{max}}^*$	305	K	Upper reference temperature for g_m	This study
$T_2\_g_m$	301	K	Upper reference temperature for g_m	Ronda et al. (2001)
u	Measured	$\mathrm{m\ s^{-1}}$	Wind speed at a reference height	This study
u_h	Calculated	$\mathrm{m\ s^{-1}}$	Wind speed at the top of canopy	Shuttleworth and Wallace (1985)
u_*	Measured	$\mathrm{m\ s^{-1}}$	Friction velocity	This study
z_m	Measured	m	Reference height of measurement	This study
z_0	Calculated	m	Roughness lengths governing the transfer of momentum	Choudhury and Monteith (1988)
$z0s$	$h_c/10$	m	Effective roughness length of soil substrate	Monteny et al. (1997)
ρ	Measured	$\mathrm{kg\ m^{-3}}$	Air density	This study
γ	0.066	$\mathrm{kPa\ K^{-1}}$	Psychrometric constant	Shuttleworth and Wallace (1985)
Γ	Calculated	$\mathrm{mg\ m^{-3}}$	CO_2 compensation point	Ronda et al. (2001)
$\Gamma(T_{sk} = 298\ \mathrm{K})$	82.2	$\mathrm{mg\ m^{-3}}$	CO_2 compensation point at 298 K	Chen et al. (2008)
θ	Measured	$\mathrm{m^3\ m^{-3}}$	Soil water content	This study

$$A = R_n - G - G_w,\tag{B9}$$

$$A_s = R_{ns} - G - G_w,\tag{B10}$$

$$R_{ns} = R_n \exp(-k_r\, LAI).\tag{B11}$$

The aerodynamic resistances r_a^a and r_a^s (s m^{-1}) are calculated by integrating the eddy diffusion coefficients from the soil surface to the level of the preferred sink of momentum in the canopy, and from there to the reference height (Shuttleworth & Gurney, 1990), respectively,

$$r_a^a = \frac{1}{ku_*} + \frac{h_c}{\kappa_m K_h}\left\{\exp\left[\kappa_m\left(1 - \frac{d_0 + z_0}{h_c}\right)\right] - 1\right\},\tag{B12}$$

$$r_a^s = \frac{h_c \exp(\kappa_m)}{\kappa_m K_h}\left\{\exp\left(\frac{-\kappa_m z_{0s}}{h_c}\right) - \exp\left[-\kappa_m\left(\frac{d_0 + z_0}{h_c}\right)\right]\right\},\tag{B13}$$

$$z_0 = \begin{cases} z_{0s} + 0.3h_c X^{1/2} & 0 < X < 0.2 \\ 0.3h_c\left(1 - \dfrac{d_0}{h_c}\right) & 0.2 < X < 1.5 \end{cases},\tag{B14}$$

$$X = C_d\, LAI,\tag{B15}$$

$$d_0 = 1.1 hc \ln(1 + X1/4),\tag{B16}$$

$$K_h = ku_*(h_c - d_0).\tag{B17}$$

The canopy boundary-layer resistance r_a^c (s m^{-1}) is calculated by integrating the leaf boundary-layer conductance over the canopy height, assuming leaf area index to be uniformly distributed with height (Choudhury & Monteith, 1988),

$$r_a^c = \frac{r_b}{2LAI},\tag{B18}$$

$$r_b = \frac{100}{\kappa_m}\left(\frac{d_l}{u_h}\right)\Big/\left[1 - \exp\left(\frac{-\kappa_m}{2}\right)\right],\tag{B19}$$

$$u_h = u/(1 + \ln(z_m - h_c + 1)).\tag{B20}$$

The soil surface resistance from interior to the surface of soil (r_s^s) is calculated using the soil water content θ (m^3 m^{-3}) and tunnel parameter f:

$$r_s^s = \exp(8.206 - 4.225 \times \theta) * f.\tag{B21}$$

This equation is modified from equation (19) of Sellers et al. (1992) by including the factor f. This factor f is used to indicate the comprehensive effects of soil salinity and soil texture on evaporation of soil water. The texture and salinity of sediments in mangrove forests have been found to affect surface evaporation, although these effects are thought to be small (Nassar & Horton, 1999; Panin & Brezgunov, 2007). Increasing salinity or highly compacted soil texture increase r_s^s and thus reduce evaporation (Nassar & Horton, 1999). The f values are tuned based on different texture types of muddy, sand, bedrock, and carbonate types in mangrove forests (Woodroffe, 1992) and a realistic range of soil salinities. The f values are determined by using a linear least-squares method to minimize differences between observed and simulated soil evaporation enthalpy fluxes. In this study, the f values in all three mangroves converge to 2. Sensitivity tests on the response of ET or T/ET to variations in f show that a variation of 1% in f causes a variation in ET of less than 0.1%. The input parameter θ was only measured at the GQ mangrove ecosystem in this study.

Appendix C: Canopy Resistance (r_s^c) in the Two-Source Model

The canopy resistance r_s^c is solved from a plant physiological approach at the leaf scale and then upscaled to the canopy scale using an analytical formulation (Ronda et al., 2001). At the leaf scale, the CO_2 stomatal conductance is described by a photosynthesis-stomatal conductance model as:

$$g_l^c = g_{min, \ c} + \frac{a_1 A_g}{(C_s - \Gamma)\left(1 + \frac{D_s}{D_0}\right)}, \tag{C1}$$

$$A_g = (A_m + R_d)\left\{1 - \exp\left(\frac{\alpha PAR}{A_m + R_d}\right)\right\}, \tag{C2}$$

$$A_m = A_{m,max}\left\{1 - \exp\left[\frac{-g_m(C_i - \Gamma)}{A_{m,max}}\right]\right\}, \tag{C3}$$

$$Rd = 0.11 Am. \tag{C4}$$

The effect of water stress on net photosynthesis and canopy conductance is accounted for by multiplying A_g by a soil moisture-dependent function:

$$Ag = Ag^* f(\theta), \tag{C5}$$

where A_g^* is the unstressed rate. The function $f(\theta)$ is given as

$$f(\theta) = 2\beta(\theta) - \beta^2(\theta), \tag{C6}$$

$$\beta(\theta) = \max\left[0, \min\left(1, \frac{\theta - WP}{FC - WP}\right)\right], \tag{C7}$$

where FC and WP are the soil moisture contents at field capacity and at permanent wilting point, respectively. The function β ranges from 1 (plants without water stress) to 0 (at wilting point). However, mangrove ecosystems are not threatened by water stress due to high FC (close to 1), so $f(\theta)$ is close to 1 in our calculations. The method to upscale g_l^c to canopy conductance g_c^c was presented by Ronda et al. (2001), who formulated canopy conductance to H_2O as $1.6 g_s^c$. Resistance is calculated as the reciprocal of conductance.

References

Allen, S. T., Reba, M. L., Edwards, B. L., & Keim, R. F. (2017). Evaporation and the subcanopy energy environment in a flooded forest. *Hydrological Processes*, *31*(16), 2860–2871.

Alongi, D. M. (2008). Mangrove forests: Resilience, protection from tsunamis, and responses to global climate change. *Estuarine, Coastal and Shelf Science*, *76*(1), 1–13.

Alongi, D. M. (2009). *The energetics of mangrove forests*. Netherlands: Springer.

Alongi, D. M. (2014). Carbon cycling and storage in mangrove forests. *Annual Review of Marine Science*, *6*, 195–219.

Alongi, D. M. (2015). The impact of climate change on mangrove forests. *Current Climate Change Reports*, *1*(1), 30–39.

Alongi, D. M., & Mukhopadhyay, S. K. (2015). Contribution of mangroves to coastal carbon cycling in low latitude seas. *Agricultural and Forest Meteorology*, *213*, 266–272.

Ball, M. C. (1988). Ecophysiology of mangroves. *Trees*, *2*, 129–142.

Ball, M. C. (1996). Comparative ecophysiology of mangrove forest and tropical lowland moist rainforest. In S. S. Mulkey, R. L. Chazdon & A. P. Smith (Eds.), *Tropical forest plant ecophysiology* (pp. 461–496). New York: Chapman and Hall.

Ball, M. C. (2002). Interactive effects of salinity and irradiance on growth: Implications for mangrove forest structure along salinity gradients. *Trees*, *16*(2-3), 126–139.

Ball, M. C., Cowan, I. R., & Farquhar, G. D. (1988). Maintenance of leaf temperature and the optimisation of carbon gain in relation to water loss in a tropical mangrove forest. *Functional Plant Biology*, *15*(2), 263–276.

Ball, M. C., & Farquhar, G. D. (1984). Photosynthetic and stomatal responses of two mangrove species, *Aegiceras corniculatum* and *Avicennia marina*, to long term salinity and humidity conditions. *Plant Physiology*, *74*(1), 1–6.

Barr, E. V., Fuentes, J. D., Zieman, J. C., O'Halloran, T. L., Smith, T. J., & Anderson, G. H. (2010). Controls on mangrove forest-atmosphere carbon dioxide exchanges in western Everglades National Park. *Journal of Geophysical Research*, *115*, G02020. https://doi.org/10.1029/2009JG001186

Barr, J. G., DeLonge, M. S., & Fuentes, J. D. (2014). Seasonal evapotranspiration patterns in mangrove forests. *Journal of Geophysical Research: Atmospheres*, *119*, 3886–3899. https://doi.org/10.1002/2013JD021083

Barr, J. G., Engel, V., Fuentes, J. D., Fuller, D. O., & Kwon, H. (2013). Modeling light use efficiency in a subtropical mangrove forest equipped with CO_2 eddy covariance. *Biogeosciences*, *10*(3), 2145–2158.

Barr, J. G., Engel, V., Smith, T. J., & Fuentes, J. D. (2012). Hurricane disturbance and recovery of energy balance, CO_2 fluxes and canopy structure in a mangrove forest of the Florida Everglades. *Agricultural and Forest Meteorology*, *153*, 54–66.

Barr, J. G., Fuentes, J. D., DeLonge, M. S., O'Halloran, T. L., Barr, D., & Zieman, J. C. (2013). Summertime influences of tidal energy advection on the surface energy balance in a mangrove forest. *Biogeosciences*, *10*(1), 501–511.

Barr, J. G., Fuentes, J. D., Engel, V., & Zieman, J. C. (2009). Physiological responses of red mangroves to the climate in the Florida Everglades. *Journal of Geophysical Research*, *114*, G02008. https://doi.org/10.1029/2008JG000843

Beck, H. E., Eric, F. W., Ming, P., Colby, K. F., Diego, G. M., van Dijk, A. I. J. M., et al. (2019). MSWEP V2 global 3-hourly 0.1° precipitation: Methodology and quantitative assessment. *Bulletin of the American Meteorological Society*, *100*(3), 473–500.

Beerling, D. J., & Franks, P. J. (2010). Plant science: The hidden cost of transpiration. *Nature*, *464*(7288), 495–496.

Berkelhammer, M., Noone, D. C., Wong, T. E., Burns, S. P., Knowles, J. F., Kaushik, A., et al. (2016). Convergent approaches to determine an ecosystem's transpiration fraction. *Global Biogeochemical Cycles*, *30*, 933–951. https://doi.org/10.1002/2016GB005392

Beven, K. (1979). A sensitivity analysis of the Penman-Monteith actual evapotranspiration estimates. *Journal of Hydrology*, *44*(3-4), 169–190.

Biber, P. D. (2006). Measuring the effects of salinity stress in the red mangrove, *Rhizophora mangle*. *African Journal of Agricultural Research*, *1*(1), 1–4.

Bjorkman, O., Demmig, B., & Andrews, T. J. (1988). Mangrove photosynthesis: Response to high-irradiance stress. *Functional Plant Biology*, *15*(2), 43–61.

Bloemen, J., Fichot, R., Horemans, J. A., Broeckx, L. S., Verlinden, M. S., Zenone, T., & Ceulemans, R. (2016). Water use of a multigenotype poplar short-rotation coppice from tree to stand scale. *Glob Change Biol Bioenergy*, *9*(2), 370–384.

Boyd, P. E., & Kohlmeyer, J. (1982). The influence of temperature on the seasonal and geographic distribution of three marine fungi. *Mycologia*, 894–902.

Brutsaert, W. (1982). The Surface Roughness Parameterization. In W. Brutsaert (Ed.), *Evaporation into the Atmosphere: Theory, History and Applications* (pp. 113–127). Dordrecht, Netherlands: Springer.

Buckley, T. N. (2005). The control of stomata by water balance. *New Phytologist*, *168*(2), 275–292.

Burgess, S. S. O., & Dawson, T. E. (2004). The contribution of fog to the water relations of *Sequoia sempervirens* (D. Don): Foliar uptake and prevention of dehydration. *Plant, Cell & Environment*, *27*(8), 1023–1034.

Cermák, J. (1989). Solar equivalent leaf area: an efficient biometrical parameter of individual leaves, trees and stands. *Tree Physiology*, *5*(3), 269–289.

Cheeseman, J. M., Herendeen, L. B., Cheeseman, A. T., & Clough, B. F. (1997). Photosynthesis and photoprotection in mangroves under field conditions. *Plant, Cell & Environment*, *20*(5), 1365–3040.

Chen, L., Tam, N. F. Y., Huang, J., Zeng, X., Meng, X., Zhong, C., et al. (2008). Comparison of ecophysiological characteristics between introduced and indigenous mangrove species in China. *Estuarine, Coastal and Shelf Science*, *79*(4), 644–652. https://doi.org/10.1016/j.ecss.2008.06.003

Chen, L., Wang, W., Zhang, Y., & Lin, G. (2009). Recent progresses in mangrove conservation, restoration and research in China. *Journal of Plant Ecology*, *2*(2), 45–54.

Chen, Y., Sun, Y., Kang, J., & Qi, Y. (2017). Phenetic correlation analysis on the spatial differentiation of mangrove landscape pattern and leaf area index at different scales. *Ecological Science*, *6*, 98–106. (in chinese)

Choi, M., Kustas, W. P., & Ray, R. L. (2012). Evapotranspiration models of different complexity for multiple land cover types. *Hydrological Processes*, *26*(19), 2962–2972.

Choudhury, B. J., & Monteith, J. L. (1988). A four-layer model for the heat budget of homogeneous land surfaces. *Quarterly Journal of the Royal Meteorological Society*, *114*(480), 373–398.

Clough, B. F., Ong, J. E., & Gong, W. K. (1997). Estimating leaf area index and photosynthetic production in canopies of the mangrove *Rhizophora apiculata*. *Marine Ecology Progress Series*, 285–292.

Clough, B. F., & Sim, R. G. (1989). Changes in gas exchange characteristics and water use efficiency of mangroves in response to salinity and vapour pressure deficit. *Oecologia*, *79*, 38–44.

Collatz, G. J., Ball, J. T., Grivet, C., & Berry, J. A. (1991). Physiological and environmental regulation of stomatal conductance, photo-synthesis and transpiration: A model that includes a laminar boundary layer. *Agricultural and Forest Meteorology*, *54*(2-4), 107–136.

Cui, X. (2018). Study on carbon sequestration capacity of typical mangrove forests and its response to environmental factors in subtropical China. PhD thesis, Tsinghua Univeristy (in Chinese).

Cui, X., Liang, J., Lu, W., Chen, H., Liu, F., Lin, G., et al. (2018). Stronger ecosystem carbon sequestration potential of mangrove wetlands with respect to terrestrial forests in subtropical China. *Agricultural and Forest Meteorology*, *249*, 71–80.

Farquhar, G. D., Wong, S. C., Evans, J. R., & Hubick, K. T. (1989). Photosynthesis and gas exchange. In H. J. Jones, T. J. Flower, & M. B. Jones (Eds.), *Plants under stress* (Vol. 39, pp. 47–69). Cambridge: Cambridge University Press.

Foken, T. (2008). The energy balance closure problem: An overview. *Ecological Applications*, *18*(6), 1351–1367.

Gilman, E., Ellison, J., & Coleman, R. (2007). Assessment of mangrove response to projected relative sea-level rise and recent historical reconstruction of shoreline position. *Environmental Monitoring and Assessment*, *124*(1-3), 105–130.

Gilman, E. L., Ellison, J., Duke, N. C., & Field, C. (2008). Threats to mangroves from climate change and adaptation options: A review. *Aquatic Botany*, *89*(2), 237–250.

Granier, A. (1987). Evaluation of transpiration in a Douglas-fir stand by means of sap flow measurements. *Tree Physiology*, *3*(4), 309–320.

Granier, A., Biron, P., Bréda, N., Pontailler, J. Y., & Saugier, B. (1996). Transpiration of trees and forest stands: Short and long-term monitoring using sapflow methods. *Global Change Biology*, *2*(3), 265–274.

Gu, L., Meyers, T., Pallardy, S. G., Hanson, P. J., Yang, B., Heuer, M., et al. (2007). Influences of biomass heat and biochemical energy storages on the land surface fluxes and radiative temperature. *Journal of Geophysical Research*, *112*, D02107. https://doi.org/10.1029/2006JD007425

Hatton, T. J., & Wu, H. I. (1995). Scaling theory to extrapolate individual tree water use to stand water use. *Hydrological Processes*, *9*(5–6), 527–540.

Haverd, V., Cuntz, M., Leuning, R., & Keith, H. (2007). Air and biomass heat storage fluxes in a forest canopy: Calculation within a soil vegetation atmosphere transfer model. *Agricultural and Forest Meteorology*, *147*(3), 125–139.

Heilman, J. L., Heinsch, F. A., Cobos, D. R., & McInnes, K. J. (2000). Energy balance of a high marsh on the Texas Gulf Coast: Effect of water availability. *Journal of Geophysical Research*, *105*(D17), 22,371–22,377.

Jacobs, C. M. J. (1994). Direct impact of atmospheric CO_2 enrichment on regional transpiration: PhD Thesis, Wageningen University.

Köstner, B., Granier, A., & Cermák, J. (1998). Sapflow measurements in forest stands: Methods and uncertainties. *Annales des Sciences Forestières*, *55*(1-2), 13–27.

Krauss, K. W., Barr, J. G., Engel, V., Fuentes, J. D., & Wang, H. (2015). Approximations of stand water use versus evapotranspiration from three mangrove forests in southwest Florida, USA. *Agricultural and Forest Meteorology*, *213*, 291–303.

Krauss, K. W., & Duberstein, J. A. (2010). Sapflow and water use of freshwater wetland trees exposed to saltwater incursion in a tidally influenced South Carolina watershed. *Canadian Journal of Forest Research*, *40*(3), 525–535.

Krauss, K. W., Duberstein, J. A., & Conner, W. H. (2015). Assessing stand water use in four coastal wetland forests using sapflow techniques: Annual estimates, errors and associated uncertainties. *Hydrological Processes*, *29*(1), 112–127.

Krauss, K. W., Lovelock, C. E., McKee, K. L., López-Hoffman, L., Ewe, S. M. L., & Sousa, W. P. (2008). Environmental drivers in mangrove establishment and early development: A review. *Aquatic Botany*, *89*(2), 105–127.

Krauss, K. W., Twilley, R. R., Doyle, T. W., & Gardiner, E. S. (2006). Leaf gas exchange characteristics of three neotropical mangrove species in response to varying hydroperiod. *Tree Physiology*, *26*(7), 959–968.

Krauss, K. W., Young, P. J., Chambers, J. L., Doyle, T. W., & Twilley, R. R. (2007). Sap flow characteristics of neotropical mangroves in flooded and drained soils. *Tree Physiology*, *27*(5), 775–783.

Kume, T., Komatsu, H., Kuraji, K., & Suzuki, M. (2008). Less than 20-min time lags between transpiration and stem sap flow in emergent trees in a Bornean tropical rainforest. *Agricultural and Forest Meteorology*, *148*(6-7), 1181–1189.

Kunert, N., Aparecido, L. M. T., Wolff, S., Higuchi, N., Jd, S., Araujo, A. C. D., & Trumbore, S. (2017). A revised hydrological model for the Central Amazon: The importance of emergent canopy trees in the forest water budget. *Agricultural and Forest Meteorology*, *239*, 47–57.

Liang, J., Wright, J. S., Cui, X., Sternberg, L., Gan, W., & Lin, G. (2018). Leaf anatomical traits determine the ^{18}O enrichment of leaf water in coastal halophytes. *Plant, Cell & Environment*, *41*(12), 2744–2757.

Limm, E. B., Simonin, K. A., Bothman, A. G., & Dawson, T. E. (2009). Foliar water uptake: A common water acquisition strategy for plants of the redwood forest. *Oecologia*, *161*(3), 449–459.

Lin, G., & Sternberg, L. S. L. (1992). Effect of growth form, salinity, nutrient and sulfide on photosynthesis, carbon isotope discrimination and growth of red mangrove (*Rhizophora mangle* L.). *Plant Physiology*, *19*, 509–526.

Liu, F. (2015). Comparison research of carbon flux and energy exchange in subtropical mangrove ecosystem. Master thesis, Tsinghua Univeristy (in Chinese).

Lloyd, J., Kriedemann, P. E., & Syvertsen, J. P. (1987). Gas exchange, water relations and ion concentrations of leaves of salt stressed 'Valencia' orange, *Citrus sinensis* (L.) Osbeck. *Functional Plant Biology*, *14*(4), 387–396.

Lopez-Hoffman, L., Anten, N. P. R., Martinez-Ramos, M., & Ackerly, D. D. (2007). Salinity and light interactively affect neotropical mangrove seedlings at the leaf and whole plant levels. *Oecologia*, *150*(4), 545–566.

Lovelock, C. E., & Ball, M. C. (2002). Influence of salinity on photosynthesis of halophytes. In A. Läuchli, & U. Lüttge (Eds.), *Salinity: Environment–plants–molecules* (pp. 315–339). Netherlands: Dordrecht Springer.

Lovelock, C. E., & Winter, K. (1996). Oxygen-dependent electron transport and protection from photoinhibition in leaves of tropical tree species. *Planta*, *198*(4), 580–558.

Lu, W. (2013). Carbon budgets in a mangrove ecosystem of Zhanjiang, Guangdong Province, China and their responses to environmental changes. PhD thesis, Xiamen University (in Chinese).

Lu, W., Xiao, J., Liu, F., Zhang, Y., Liu, C., & Lin, G. (2017). Contrasting ecosystem CO_2 fluxes of inland and coastal wetlands: A meta-analysis of eddy covariance data. *Global Change Biology*, *23*(3), 1180–1198.

Mezbahuddin, M., Grant, R. F., & Flanagan, L. B. (2016). Modeling hydrological controls on variations in peat water content, water table depth and surface energy exchange of a boreal western Canadian fen peatland. *Journal of Geophysical Research: Biogeosciences*, *121*, 2216–2242. https://doi.org/10.1002/2016JG003501

Monteny, B. A., Lhomme, J. P., Chehbouni, A., Troufleau, D., Amadou, M., Sicot, M., et al. (1997). The role of the Sahelian biosphere on the water and the CO_2 cycle during the HAPEX-Sahel experiment. *Journal of Hydrology*, *188-189*, 516–535.

Muller, E., Lambs, L., & Fromard, F. (2009). Variations in water use by a mature mangrove of *Avicennia germinans*, French Guiana. *Annals of Forest Science*, *66*(8), 803–813.

Nassar, I. N., & Horton, R. (1999). Salinity and compaction effects on soil water evaporation and water and solute distributions. *Soil Science Society of America Journal*, *63*(4), 752–758.

Nguyen, H. T., Stanton, D. E., Schmitz, N., Farquhar, G. D., & Ball, M. C. (2015). Growth responses of the mangrove *Avicennia marina* to salinity: Development and function of shoot hydraulic systems require saline conditions. *Annual Botany*, *115*(3), 397–407.

Oren, R., Sperry, J. S., Katul, G. G., Pataki, D. E., Ewers, B. E., Phillips, N., & Schäfer, K. V. R. (1999). Survey and synthesis of intra- and interspecific variation in stomatal sensitivity to vapour pressure deficit. *Plant, Cell & Environment*, *22*(12), 1515–1526.

Osmond, C. B. (1994). What is photoinhibition? Some insights from comparisons of shade and sun plants. In N. R. Baker & J. R. Bowyer (Eds.), *Photoinhibition of Photosynthesis from Molecular Mechanisms to the Field* (pp. 1–24). Oxford, UK: BIOS Sci. Publ. Ltd.

Panin, G. N., & Brezgunov, V. S. (2007). Influence of the salinity of water on its evaporation. *Izvestiya, Atmospheric and Oceanic Physics*, *43*(5), 663–665.

Parida, A. K., Das, A. B., & Mittra, B. (2004). Effects of salt on growth, ion accumulation, photosynthesis and leaf anatomy of the mangrove, *Bruguiera parviflora*. *Trees*, *18*(2), 167–174.

Quisthoudt, K., Schmitz, N., Randin, C. F., Dahdouh-Guebas, F., Robert, E. M. R., & Koedam, N. (2012). Temperature variation among mangrove latitudinal range limits worldwide. *Trees*, *26*(6), 1919–1931.

Reef, R., & Lovelock, C. E. (2015). Regulation of water balance in mangroves. *Annals of Botany*, *115*(3), 385–395.

Reef, R., Schmitz, N., Rogers, B. A., Ball, M. C., & Lovelock, C. E. (2012). Differential responses of the mangrove *Avicennia marina* to salinity and abscisic acid. *Functional Plant Biology*, *39*(12), 1038.

Ronda, R. J., De Bruin, H. A. R., & Holtslag, A. A. M. (2001). Representation of the canopy conductance in modeling the surface energy budget for low vegetation. *Journal of Applied Meteorology*, *40*(8), 1431–1444.

Ross, J. (1981). *The radiation regime and architecture of plant stands*. Netherlands: Springer.

Sellers, P. J., Heiser, M. D., & Hall, F. G. (1992). Relations between surface conductance and spectral vegetation indices at intermediate (100 m^2 to 15 km^2) length scales. *Journal of Geophysical Research*, *97*(D17), 19,033–19,059.

Shoemaker, W. B., Sumner, D. M., & Castillo, A. (2005). Estimating changes in heat energy stored within a column of wetland surface water and factors controlling their importance in the surface energy budget. *Water Resources Research*, *41*, W10411. https://doi.org/10.1029/2005WR004037

Shuttleworth, W. J. (1988). Evaporation from Amazonian rainforest. *Royal Society of London.series B Biological Sciences*, *233*, 321–346.

Shuttleworth, W. J., & Gurney, R. J. (1990). The theoretical relationship between foliage temperature and canopy resistance in sparse crops. *Quarterly Journal of the Royal Meteorological Society*, *116*(492), 497–519.

Shuttleworth, W. J., & Wallace, J. S. (1985). Evaporation from sparse crops—An energy combination theory. *Quarterly Journal of the Royal Meteorological Society*, *111*(469), 839–855.

Si, H. T., Yu, T. H., Guan, X. Y., Jiang, G. F., & Cao, K. F. (2017). Stomatal responses to environmental factors and its coordination with hydraulic functions in plants of mangrove forests. *Plant Physiology Journal*, *53*(3), 487–496.

Sobrado, M. A. (2000). Relation of water transport to leaf gas exchange properties in three mangrove species. *Trees*, *14*(5), 258–262.

Sobrado, M. A. (2005). Leaf characteristics and gas exchange of the mangrove *Laguncularia racemosa* as affected by salinity. *Photosynthetica*, *43*(2), 217–221.

Sobrado, M. A. (2007). Relationship of water transport to anatomical features in the mangrove *Laguncularia racemosa* grown under contrasting salinities. *New Phytologist*, *173*(3), 584–591.

Sobrado, M. A., & Ball, M. C. (1999). Light use in relation to carbon gain in the mangrove, *Avicennia marina*, under hypersaline conditions. *Functional Plant Biology*, *26*(3), 245–251.

Soegaard, H., & Boegh, E. (1995). Estimation of evapotranspiration from a millet crop in the Sahel combining sap flow, leaf area index and eddy correlation technique. *Journal of Hydrology*, *166*(3–4), 265–282.

Tan, Z. H., Zhang, Y. P., Deng, X. B., Song, Q. H., Liu, W. J., Deng, Y., et al. (2015). Interannual and seasonal variability of water use efficiency in a tropical rainforest: Results from a 9 year eddy flux time series. *Journal of Geophysical Research: Atmospheres*, *120*, 464–479. https://doi.org/10.1002/2014JD022535

Tanaka, Y., Sugano, S. S., Shimada, T., & Hara-Nishimura, I. (2013). Enhancement of leaf photosynthetic capacity through increased stomatal density in *Arabidopsis*. *The New Phytologist*, *198*(3), 757–764.

Twine, T. E., Kustas, W. P., Norman, J. M., Cook, D. R., Houser, P., Meyers, T. P., et al. (2000). Correcting eddy-covariance flux underestimates over a grassland. *Agricultural and Forest Meteorology*, *103*(3), 279–300.

Vertessy, R. A., Benyon, R. G., O'Sullivan, S. K., & Gribben, P. R. (1995). Relationships between stem diameter, sapwood area, leaf area and transpiration in a young mountain ash forest. *Tree Physiology*, *15*(9), 559–567.

von Caemmerer, S., & Evans, J. R. (2015). Temperature responses of mesophyll conductance differ greatly between species. *Plant, Cell & Environment*, *38*(4), 629–637.

Wang, L., Good, S. P., & Caylor, K. K. (2014). Global synthesis of vegetation control on evapotranspiration partitioning. *Geophysical Research Letters*, *41*, 6753–6757. https://doi.org/10.1002/2014GL061439

Wang, L., Niu, S., Good, S. P., Soderberg, K., McCabe, M. F., Sherry, R. A., et al. (2013). The effect of warming on grassland evapotranspiration partitioning using laser-based isotope monitoring techniques. *Geochimica et Cosmochimica Acta*, *111*, 28–38.

Wang, W., Yan, Z., You, S., Zhang, Y., Chen, L., & Lin, G. (2011). Mangroves: Obligate or facultative halophytes? A review. *Trees*, *25*(6), 953–963.

Wei, Z., Lee, X., Wen, X., & Xiao, W. (2018). Evapotranspiration partitioning for three agro-ecosystems with contrasting moisture conditions: A comparison of an isotope method and a two-source model calculation. *Agricultural and Forest Meteorology*, *252*, 296–310.

Wei, Z., Yoshimura, K., Wang, L., Miralles, D. G., Jasechko, S., & Lee, X. (2017). Revisiting the contribution of transpiration to global terrestrial evapotranspiration: Revisiting global *ET* partitioning. *Geophysical Research Letters*, *44*, 2792–2801. https://doi.org/10.1002/2016GL072235

Wen, Y. (1999). Biomass and productivity of five mangrove communities in Yingluo Bay of Guangxi. *Guangxi Sciences*, *6*(2), 142–147.

Wilson, K., Goldstein, A., Falge, E., Aubinet, M., Baldocchi, D., Berbigier, P., et al. (2002). Energy balance closure at FLUXNET sites. *Agricultural and Forest Meteorology*, *113*(1), 223–243.

Woodroffe, C. (1992). Mangrove sediments and geomorphology. In A. I. Robertson & D. M. Alongi (Eds.), *Tropical mangrove ecosystems* (pp. 225–249). Washington, DC: American Geophysical Union.

Xiao, J., Sun, G., Chen, J., Chen, H., Chen, S., Dong, G., et al. (2013). Carbon fluxes, evapotranspiration, and water use efficiency of terrestrial ecosystems in China. *Agricultural and Forest Meteorology*, *182-183*, 76–90. https://doi.org/10.1016/j.agrformet.2013.08.007

Yan, G. Y., Feng, J. X., Yang, S. C., & Lin, G. H. (2016). Sapflow characteristics of *Kandelia obovata* and their controlling factors in Zhangjiang estuary, China. *Journal of Applied Ecology (in Chinese)*, *27*(7), 2048–2058.